

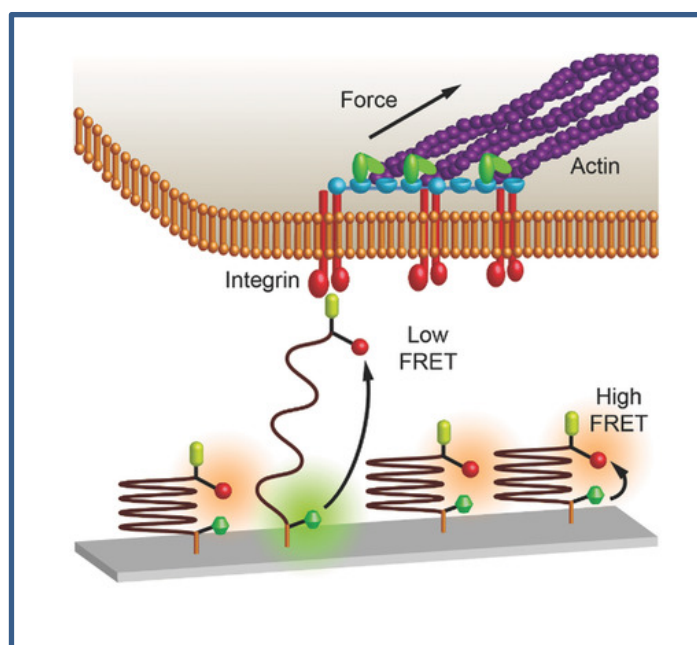


Published in final edited form as:

Göktas, M., & Blank, K. G. (2017). Molecular Force Sensors: From Fundamental Concepts toward Applications in Cell Biology. *Advanced Materials Interfaces*, 4(1): 1600441. doi:10.1002/admi.201600441.

Molecular force sensors: from fundamental concepts towards applications in cell biology

Melis Goktas, Kerstin G. Blank



See the force: Cellular mechanotransduction is a complex process that involves many different molecular interactions. The forces acting between these molecules are largely unknown. This progress report summarizes recent advances in the development of molecular force sensors. These molecular building blocks, which convert a mechanical signal into an optical readout, shed light on the mechanical aspects of this process.

DOI: 10.1002/ ((please add manuscript number))

Article type: Progress Report

Molecular force sensors: from fundamental concepts towards applications in cell biology

*Melis Goktas, Kerstin G. Blank**

MSc M. Goktas, Dr. K. G. Blank

Max Planck Institute of Colloids and Interfaces, Mechano(bio)chemistry

Science Park Potsdam-Golm

14424 Potsdam

Germany

E-mail: Kerstin.Blank@mpikg.mpg.de

Keywords

mechanosensing; mechanotransduction; focal adhesions; extracellular matrix; molecular force sensors

Abstract

Mechanical signals are central for the regulation of developmental, physiological and pathological processes within biological systems. Force transduction across the cell-extracellular matrix (ECM) interface is highly crucial for regulating cell fate *via* mechanosensing and mechanotransduction cascades. The key molecules involved in these highly sophisticated processes have been identified in recent years. But little is still known about their interactions, and in particular the molecular forces that determine these interactions. This is due to the limited availability of techniques that allow for investigating force propagation and mechanobiochemical signal conversion at the molecular level in live cells. In this progress report, currently available tools for measuring the molecular forces involved in cellular mechanosensing and mechanotransduction are summarized, specifically highlighting recent advances in the development of molecular force sensors (MFSs). MFSs convert the applied force into a fluorescence signal, allowing for a direct readout of tension with optical microscopy techniques. Moving from molecular design principles to applications of MFSs, important results are summarized, highlighting the new mechanistic information that has been obtained about mechanobiochemical processes at the cell-ECM interface. This progress report finishes with a critical discussion of current promises and limitations, providing perspectives for future research in this quickly evolving field.

1. Introduction

The molecular machinery of cells utilizes a large variety of intracellular mechanosensors and actuators to control processes such as cell movement, cell division, vesicle transport as well as membrane shaping and fusion.^[1] In addition to this intracellular machinery, specific receptor–ligand interactions between cells and their extracellular environment are involved in the mechanoregulation of cellular processes. Mechanical signals, *i.e.* forces, are constantly transmitted from the extracellular to the intracellular side and *vice versa*, allowing cells to probe the physical properties of their surroundings.^[2-4] The perceived mechanical information is translated into biochemical activity and serves as input for intracellular signaling cascades in a process called mechanotransduction.^[4-7] Receptor-mediated force transduction regulates many cellular processes such as adhesion,^[8] migration,^[9] proliferation,^[10] differentiation^[11] as well as tumor formation and progression.^[12] Whereas receptor-based mechanotransduction mechanisms are universal to a larger number of cell types, also highly specialized processes have evolved that allow biological systems to sense and process mechanical signals. Examples are the muscle protein titin kinase^[13,14] and the vascular protein von Willebrand factor.^[15,16] Both proteins have important regulatory function in their respective tissues, possessing cryptic functional sites that become exposed upon stretching.

Focusing on the general mechanism of receptor-mediated force transduction, a detailed molecular picture is required for understanding the highly sophisticated response of cells to different physical parameters in their environment, such as geometry and material properties. Proteomic studies have allowed for identifying a larger number of proteins involved in these mechanotransduction cascades^[17] and it is now widely accepted that many of these proteins undergo force-induced conformational changes that alter their activity.^[2,3,7] Little is known, however, about the magnitude of the molecular forces that are required for triggering these conformational changes. Knowledge of the molecular forces is of fundamental importance for establishing structure-function-mechanics relationships of these mechanoactive proteins and for understanding diseases that involve malfunctioning mechanotransduction cascades, such as arteriosclerosis, muscular dystrophies, osteoporosis, developmental disorders and cancer.^[18] The molecular forces acting between cell-surface receptors and their extracellular binding partners are further crucial input for designing synthetic materials that mimic the physical properties of the natural extracellular environment.

In this progress report, we first provide a short overview of the cellular structures responsible for transmitting forces between the intracellular and the extracellular environment. We then introduce the methods that have been developed for measuring these forces, with a special focus on molecular force sensors (MFSs). Several excellent reviews have appeared recently, focusing mostly on the applications of MFSs in cell biology.^[7,19-22] Here, we take a molecular point of view with the aim of categorizing currently used MFSs by their working mechanism. Focusing on common principles, we critically discuss how molecular mechanical information can be obtained and how the results obtained from MFS measurements compare to other techniques. In this context, we further highlight the need for new MFS designs that span a larger force range and discuss general biophysical concepts that determine the functionality of MFSs.

2. Mechanosensing and mechanotransduction at focal adhesions

The key mechanical link between intracellular and extracellular structures is established *via* focal adhesions (FAs). These complex, hierarchical assemblies of proteins directly connect the cytoskeleton with the extracellular matrix (ECM). Within these assemblies, integrins mediate the primary cell-ECM linkage (**Figure 1**).^[7,23-25] Integrins are transmembrane proteins composed of one α and one β subunit, forming a heterodimer. In mammals, 18 different α and 8 different β subunits are found, which can assemble into 24 different heterodimers.^[26] The α subunit determines the specificity of the cell-ECM interaction, while the β subunit provides attachment of the heterodimer to the actin cytoskeleton *via* adaptor proteins.^[27] Depending on their specificity, integrins mediate cell adhesion to a variety of ECM proteins such as fibronectin, collagen, laminin and vitronectin.^[28,29] Besides differences in specificity, also the binding affinity and signaling activity of integrin heterodimers varies. For example, both $\alpha_v\beta_3$ and $\alpha_5\beta_1$ integrins are involved in mechanotransduction, but their specific roles are still not fully understood.^[30,31] On the intracellular side, focal adhesions consist of a large number of different structural and signaling proteins, including adaptor proteins that link the integrin receptors to the actin cytoskeleton. Talin is the primary adaptor protein that has multiple binding domains for both F-actin and β -integrin domains, thereby establishing a direct linkage between integrins and the cytoskeleton. Other structural adaptor proteins that connect F-actin and β -integrin domains include α -actinin, filamin and tensin.^[3,32]

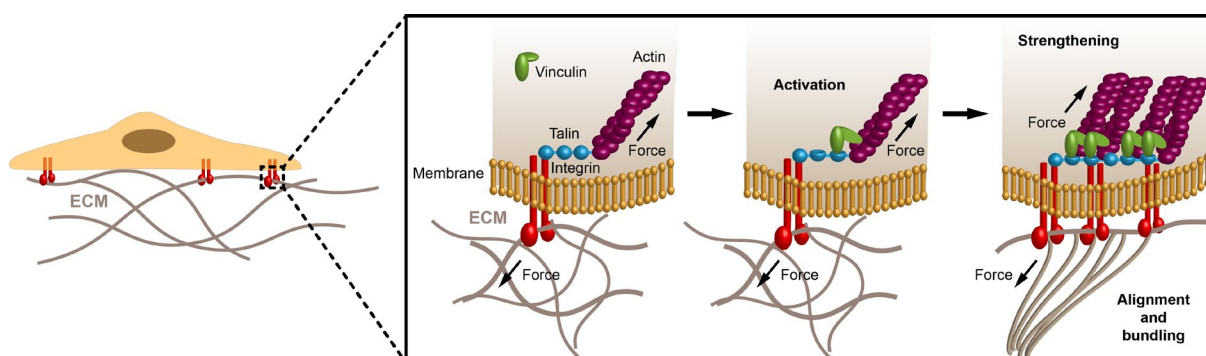


Figure 1. Mechanotransduction *via* focal adhesions (FAs). Cells adhere to ECM ligands *via* integrin receptors. Following integrin activation, talin is recruited at the intracellular side where it forms the link between integrins and the actin cytoskeleton. After the formation of integrin-actin bridges, forces transmitted *via* the FAs cause conformational changes in talin. Mechanically stretched talin exposes cryptic binding sites for vinculin, a protein that provides additional links to actin. This critical step ensures stress fiber formation and FA strengthening.

Focal adhesions are highly dynamic structures that form in a sequence of steps.^[7,24,25] Integrin receptors present in cellular lamellipodia at the leading edge of the cell bind to integrin ligands in the ECM. The following steps are not fully understood but, most likely, involve the recruitment of adaptor proteins that allow for the formation of integrin-actin bridges. As a result, forces are applied on the adhesion sites by actin retrograde flow. These forces cause conformational changes in talin, leading to the exposure of cryptic binding sites for vinculin, thereby reinforcing the actin linkage.^[33] Over time these initial focal adhesions are translocated towards the lamellum of the cell. At this point, myosin gets engaged with actin and actin stress fibers form. Now, forces acting on these mature focal adhesions originate

from actin-myosin contractility. At this stage, several other mechanosensitive molecules become activated, allowing the further recruitment of proteins to strengthen the actin-FA linkage. All these mechanical connections are highly dynamic and reversible in the presence of the applied force, leading to a high turnover of FA proteins.

FAs do not only consist of proteins that are directly involved in establishing the mechanical linkage between the ECM and the actin network of the cell. They also contain a large number of mechanosensitive kinases and phosphatases such as receptor-like protein tyrosine phosphatase- α (RPTP $_{\alpha}$), Src family kinases and focal adhesion kinase (FAK).^[34-36] These proteins provide a direct link to the biochemical signaling pathways of the cell, *e.g.* *via* Rho family GTPases and the MAP kinase pathway, ultimately regulating gene expression. It is further known that mechanical forces transmitted *via* the cytoskeleton propagate to the nucleus, most likely promoting structural rearrangements and altering gene accessibility.^[37-40] The fact that cells possess several types of FAs that are connected with the cytoskeleton in different ways^[7,41] suggests that the forces transmitted *via* these structures are heterogeneous. The high dynamics of these structures may further affect the nature and stoichiometry of the FA-actin linkage. Bonds may break and reform quickly over time, thereby redirecting the pathway of the force in the FA protein assembly. This situation becomes even more complicated when considering the different binding affinities of integrin subclasses and the fact that some integrins are able to form catch bonds, *i.e.* strengthen under load.^[42,43] Taken together, the complex interplay of different FA components in cellular mechanotransduction pathways clearly highlights the need for directly measuring the forces involved in this process at the molecular level.

3. Single-cell and single-molecule force spectroscopy

Methods for measuring the forces involved in cell adhesion were already developed long before the complex architecture of FAs was established. These methods can roughly be categorized into approaches using isolated cells or purified cell-surface receptors, termed single-cell (SCFS) and single-molecule (SMFS) force spectroscopy, respectively (**Figure 2**).

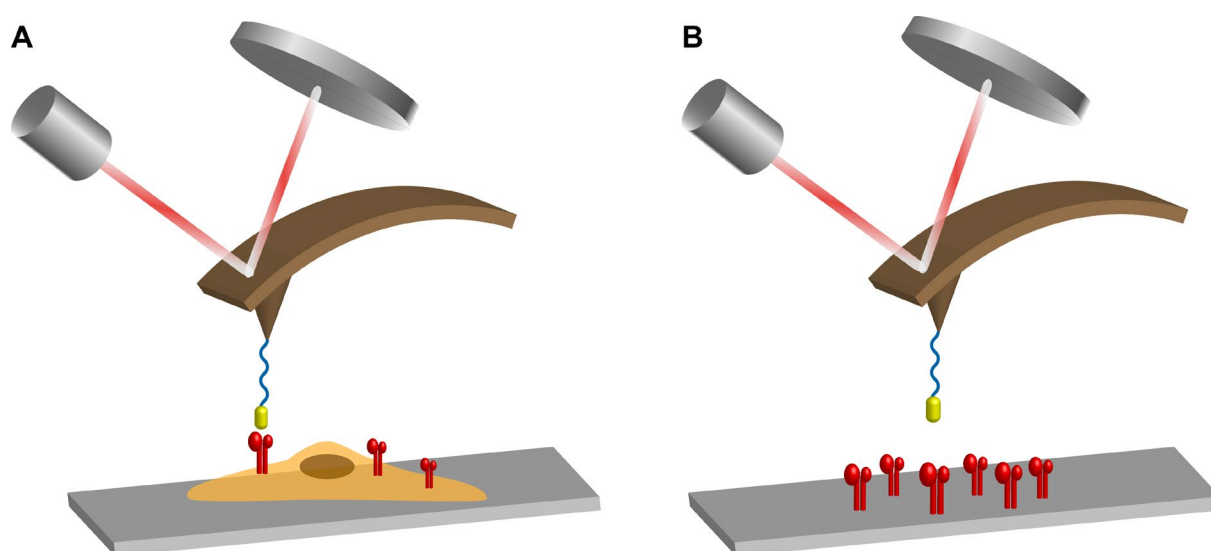


Figure 2. Force spectroscopy approaches for quantifying the forces involved in cell adhesion. (A) Single-cell force spectroscopy (SCFS). In the example shown, the tip of an

AFM cantilever is functionalized with cell-binding ligands. To measure adhesion forces, the tip is brought into contact with a cell that adheres to a substrate. **(B)** Single-molecule force spectroscopy (SMFS). The rupture forces between purified cell-surface receptors and small cell-binding ligands or full-length ECM proteins are measured.

The first SCFS method that was developed for quantifying the intermolecular forces involved in cell adhesion utilized micropipettes.^[44,45] This well-known cell-manipulation tool allows for picking up and immobilizing an individual cell *via* micropipette suction. The immobilized cell is then brought into contact with a functionalized surface or another cell that adheres to a substrate. Once adhesive contacts have formed, the micropipette is retracted and the adhesion forces are determined. Using the biomembrane force-probe approach, forces ranging from 10^{-2} -100 pN can be detected.^[45] Subsequently, other force spectroscopy techniques such as optical tweezers (~ 0.1 -100 pN force range) and magnetic tweezers ($\sim 10^{-3}$ - 10^4 pN force range) were also used for SCFS measurements.^[5,46-49] Among all of these techniques, atomic force microscopy (AFM)-based SCFS is the most versatile method for measuring cell adhesion forces due to its large range of detectable forces (~ 10 - 10^6 pN) and superior spatial (~ 1 nm to 100 μ m) and temporal (~ 0.1 s to >10 min) resolution.^[50-53] The AFM further provides the possibility of ramping up the force that acts on a molecular interaction with different rates (*i.e.* loading rates $r = dF/dt$; see **section 7.2** for a more detailed description of the importance of the loading rate).

AFM-based SCFS allows for two basic configurations. The cell, which is adhered to a substrate, is probed with an AFM cantilever that is modified with cell-binding ligands (**Figure 2A**). These ligands are coupled to the tip either directly or *via* a micrometer-sized bead attached to a tip-less cantilever. Even though easy to implement, this setup has several disadvantages such as contamination of the functionalized cantilever with cellular material during long measurements. Also, differences in the spreading area and polarization of cells on the surface affect the local density of cell-surface receptors.^[52] The preferred strategy is to attach a single cell to the AFM cantilever. The cell is then brought into contact with a substrate that contains either cell-binding ligands or another cell.^[54] This strategy eliminates possible differences in the local density of cell-surface receptors as cell spreading on the cantilever is prevented by the size and shape of the cantilever. It can further be controlled using locally functionalized cantilevers that direct cell attachment to pre-defined areas.^[52]

All SCFS experiments have in common that the number and specificity of the receptor ligand interactions formed between the cell and the substrate cannot be fully controlled. For example, different integrins can bind to the same ligand and full-length ECM proteins possess more than one integrin-binding site. This leads to rather complicated force-distance curves that contain many overlapping events. These force-distance curves further contain a contribution from the viscoelastic response of the cell body, which has been described with a number of different mechanical models.^[53] Even though it is still a challenge to interpret the force signature, it is often possible to extract the desired information when comparing force-distance curves measured in the presence and absence of specific blocking agents (*e.g.* freely soluble ligands to block one specific receptor).

Using an AFM cantilever functionalized with a linear GRGDSP peptide, the adhesion forces between this peptide and integrins expressed by osteoclasts were measured. As osteoclast

cells mainly express $\alpha_v\beta_3$ integrins,^[55,56] it can be assumed that the measured rupture force of ~ 42 pN corresponds to the interaction between a single $\alpha_v\beta_3$ integrin and the GRGDSP peptide (retract velocity between 1-50 $\mu\text{m/s}$).^[57] Later on, many research groups used SCFS for other cell lines and a variety of ligands were used for investigating the adhesion forces of other types of integrin receptors. Examples include collagen I and collagen IV coated substrates used for measuring the adhesion forces to $\alpha_2\beta_1$ integrins of Chinese hamster ovary (CHO) cells,^[58] fibronectin coated substrates for probing the adhesion to $\alpha_5\beta_1$ integrins of K562 cells,^[59] as well as vascular cell adhesion molecule-1 (VCAM-1) functionalized substrates for measuring the adhesion forces to $\alpha_4\beta_1$ integrins of U937 cells.^[60,61] These studies demonstrated a broad range of rupture forces ranging from 20 pN up to ~ 140 pN depending on the loading rate and the specific integrin-ligand interaction probed (**Table 1**).

Table 1. Integrin-ligand forces measured using single cell force spectroscopy (SCFS) and single molecule force spectroscopy (SMFS)

Method	Integrin	Ligand	Force Range (pN)	Loading Rate Range (pN/s)	References
SCFS	$\alpha_2\beta_1$	Collagen	38-90	180-8,800	[58]
SCFS	$\alpha_5\beta_1$	Fibronectin	40-140	20-50,000	[59]
SCFS	$\alpha_4\beta_1$	VCAM-1	20-175	100-100,000	[60]
SMFS	$\alpha_4\beta_1$	VCAM-1	40-175	150-100,000	[60]
SMFS	$\alpha_5\beta_1$	GRGDSP	15-109	1,000-305,000	[62]
SMFS	$\alpha_{IIb}\beta_3$	Fibrinogen	20-120	160-16,000	[63]

Molecular forces acting between cell-surface receptors and their ligands have also been determined using AFM-based SMFS (**Figure 2B**). In this case, purified receptors (or ligands) are immobilized to the AFM cantilever and probed against their respective binding partners on the substrate. After a certain contact time, allowing the receptor-ligand interaction to form, the tip is retracted from the surface until the receptor-ligand bond ruptures. The rupture force is then directly extracted from the recorded force-distance curves. Using purified receptors allows for more control over receptor density and facilitates well-defined single-molecule experiments.

A number of different integrin–ligand couples have been analyzed with SMFS, including $\alpha_5\beta_1$ –GRGDSP peptide,^[62] $\alpha_4\beta_1$ –VCAM-1^[60] and $\alpha_{IIb}\beta_3$ –fibrinogen.^[63] Similar to the SCFS measurements described above, also these measurements yielded a range of rupture forces (up to ~ 175 pN), depending on the loading rate used (**Table 1**). Even though highly powerful, the main concern with SMFS is that cell adhesion molecules are measured isolated from their natural biological context. Considering the recently obtained knowledge about FAs and their many levels of regulation, it appears likely that the removal of these molecules from their native environment might affect their conformation and consequently their functional properties.^[64]

Overall, force spectroscopy measurements allow for quantitatively probing single receptor–ligand interactions, although some limitations still exist. Both SCFS and SMFS are time

consuming and probe the interaction under highly artificial conditions. Even when performing measurements with live cells, only a small area on the surface (*i.e.* the contact area with the cantilever) is exposed to the ligand, stimulating the cell only locally. In their natural environment cells are exposed to ligands and mechanical stimuli in all three dimensions, however. In addition, thermal drift of the AFM cantilever limits the possible contact time to several minutes so that, at best, only the first steps of FA formation can be investigated. AFM measurements further lack the possibility to directly observe the location and dynamics of FA structures and stress fibers, so that efforts have been undertaken to combine AFM with fluorescence microscopy.^[48,49,65,66]

4. Traction force microscopy

Considering the limitations of SCFS and SMFS, another approach is needed for observing cells optically while they mechanically interact with their surroundings. Traction force microscopy (TFM) provides a powerful solution (**Figure 3**).^[22] In TFM experiments, cells are seeded on an elastic substrate that is meant to mimic the mechanical properties of the ECM. Cell-generated forces deform the substrate and the magnitude, direction and localization of the deformation can be observed with a simple optical microscope. Using a substrate that possesses well-characterized elastic properties, the forces can be directly calculated from the deformation. As the basic readout principle is optical, the mechanical experiment can be directly combined with fluorescence microscopy techniques. This allows for the visualization of cellular structures, in particular FAs that have formed at the interface with the elastic substrate.

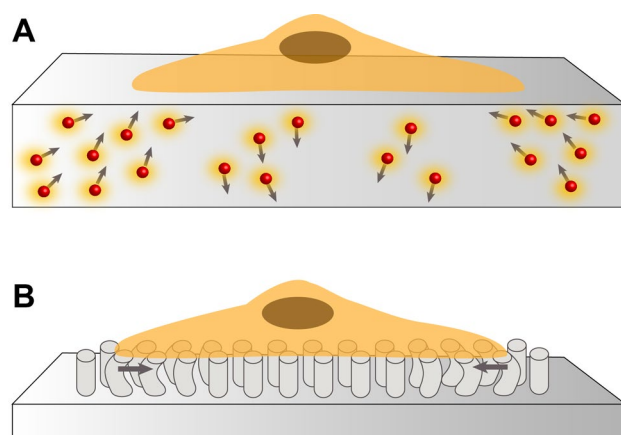


Figure 3. Traction force microscopy. (A) Cells are grown on flat elastic substrates that contain fluorescent beads randomly dispersed inside the material. Cellular traction forces are measured as a function of bead displacement. (B) Micropillar array detectors (mPADs) utilize 3D structures that display micrometer-sized elastic pillars. Cells grown on these 3D structures form FAs on top of these pillars. Cellular traction forces lead to pillar bending.

In the very first TFM experiment, cells were grown on a thin, elastic film of crosslinked silicone located on the surface of liquid silicone oil.^[67] Wrinkling of the film was observed in the surroundings of the cells and it was concluded that cells indeed apply forces on their substrate. Due to the wrinkling behavior of the thin film, it was only possible to semi-quantitatively analyze the data with elasticity theory. To improve the assay readout,

fluorescent latex beads were embedded into a pre-stressed film and the bead movement was followed to detect material deformation (**Figure 3A**).^[68] This approach allowed for the first quantitative analysis of traction forces exerted by keratocytes on the elastic substrate and the maximum cellular traction forces were estimated to be $\sim 20,000$ pN.

In later experiments, the non-functionalized, hydrophobic silicone substrate was replaced with other elastic substrates such as polyacrylamide (PAA) hydrogels, which are easier to functionalize with cell-binding ligands.^[69] Combining bead imaging with the detection of fluorescently labeled FA proteins allows for correlating cellular structures with the locations of traction force generation.^[70] Using a confocal microscope, bead displacement in the substrate can be observed in 3D and both in-plane (x,y) and normal (z) forces can be determined.^[71,72] It was shown that 3T3 fibroblasts exert traction forces of $\sim 2,000$ - $5,000$ pN/ μm^2 at the rear end of the cell. It was further observed that cells apply force in all three dimensions equally and that these forces travel into the substrate for a distance of at least $10 \mu\text{m}$.^[71]

One key advantage of using PAA for these bead-displacement experiments is the possibility of tuning the substrate stiffness within the physiologically relevant range (100 Pa – 100 kPa).^[73] It has been shown that cellular mechanotransduction mechanisms are affected by the stiffness of the substrate^[11,73] and PAA has become a frequently used material for investigating this interplay between substrate stiffness and cellular behavior. It is crucial to keep in mind, however, that PAA gels of different stiffness possess a different crosslink density and consequently also different pore sizes and slightly different chemical compositions. It is therefore difficult to discriminate between all these effects. In addition, unlike the native ECM, synthetic materials like silicone and PAA are not cleavable by cellular proteases. Recent studies utilizing fluorescent beads embedded into enzyme (*e.g.* matrix metalloprotease) cleavable matrices have shown that degradation and remodeling of the ECM affects the traction force profile of cells.^[74] Enzyme cleavable matrices were shown to support high degrees of cell spreading and higher traction forces, while matrices restricting cell-mediated degradation exhibited low degrees of spreading leading and low traction forces.

TFM based on micropillar array detectors (mPADs) utilizes a different strategy to alter the elastic properties of the substrate. The micrometer-sized pillars of an mPAD array are arranged in 3D-structures (**Figure 3B**) made from polydimethylsiloxane (PDMS). Instead of adjusting the crosslink density, the pillar height and diameter are altered to vary the mechanical properties that affect the cells.^[75] Frequently, the top of the pillars is coated with cell-binding ligands (*e.g.* fibronectin, collagen) to guide cell attachment to the top of each micropillar.^[75] Visualizing the FA protein vinculin with a fluorescently labeled antibody, it was shown that cellular traction forces were positively correlated with the size of FAs once FA size was larger than $1 \mu\text{m}^2$. Some smaller adhesion sites generated disproportionately high forces and it was suggested that these sites resemble earlier adhesion complexes that are not yet fully matured. Further investigations demonstrated that the relationship between force and focal adhesion area is not constant, but depends on substrate stiffness. Depending on the size of an FA (~ 2 - $5 \mu\text{m}^2$), REF52 fibroblasts generated forces varying from 3,000 up to $\sim 80,000$ pN within a stiffness range from 4,700 up to $80,000$ pN/ μm^2 .^[76]

A large number of TFM experiments have contributed to our knowledge of the magnitude of forces acting at the cell-matrix interface. The strength of TFM clearly lies in the possibility of

visualizing cellular structures so that the size of FAs can be determined easily together with the traction forces applied *via* these structures. It needs to be considered, however, that the spatial resolution is limited to a few micrometers and that many receptor-ligand interactions contribute to the measured displacement. As a consequence, the measured traction forces are usually in the nanonewton (nN) range, which is significantly higher than the receptor-ligand forces determined with SCFS or SMFS.^[58-60,62,63] Without a detailed knowledge of the exact number of receptor–ligand bonds formed at a given moment in time, no information about the single-molecular forces can be obtained. Attempts have been made to estimate the number of integrin molecules within one focal adhesion and, consequently, the force acting on one single integrin molecule. The calculated forces range from 1 pN^[77] to 30 pN,^[3] clearly showing that such estimates are complicated by the highly dynamic nature of FAs where only a small fraction of integrins may be actively involved in force transmission. This is supported by the forces measured with SCFS and SFMS, which span a range from 15-175 pN (**Table 1**), suggesting that the forces acting on individual integrins may be higher than the forces estimated from TFM experiments. These discrepancies within one technique and between different techniques again highlight the need for new tools that allow for measuring single-molecular forces directly at the cell-matrix interface.

5. First-generation molecular force sensors

The ideal technique for quantifying cell-matrix forces combines the advantages of SCFS/SMFS and TFM. It requires single-molecule force resolution as well as the possibility of observing many individual interactions simultaneously, ideally using a fluorescence readout. We have already proposed in 2003 that individual molecules can be utilized as highly sensitive force sensors.^[78] Equipped with a fluorescence readout, these molecular force sensors (MFSs) are sensitive probes that can be used to observe mechanical processes in a highly parallel fashion using a simple optical readout. When introducing this principle, the initial goal was to improve the force resolution of SMFS techniques, which is ultimately limited by thermal fluctuations acting on the AFM cantilever and magnetically or optically trapped beads.^[79] It is known that the size of the force probe directly affects the magnitude of thermal fluctuations.^[80] Depending on the size of the AFM cantilever, the force resolution is usually between 5-10 pN and cannot be reduced any further due to limitations in the methods employed for cantilever microfabrication. It appeared to be a logical conclusion to use an individual molecule instead, *i.e.* the smallest possible force sensor.

To investigate the feasibility of replacing a macroscopic force sensor with a single molecule, we have replaced the AFM cantilever with a short DNA duplex as a model MFS (**Figure 4A**). DNA is mechanically well-characterized and the rupture forces of short double-stranded DNA (dsDNA) molecules can be tuned easily depending on their length,^[81-83] sequence^[84,85] and pulling geometry.^[85-88] To implement dsDNA as a MFS, a so-called differential force assay (DFA) was developed where two different dsDNA molecules were directly compared with each other in a molecular tug-of-war.^[78,79] Both DNA duplexes under investigation were connected *via* a linker that carried a fluorescent label. This molecular chain was coupled to a glass surface at one end and to an elastic PDMS surface on the other end. When separating the two surfaces, the force acting on the molecular chain builds up until the weaker bond ruptures. For an individual molecular chain, the stronger bond breaks with a lower probability and the

fluorescent label remains on the surface containing the stronger bond. In a real experiment, a large number of individual chains are tested simultaneously and the fluorescence intensity on both surfaces provides a direct readout of the relative stability of the two dsDNA molecules.

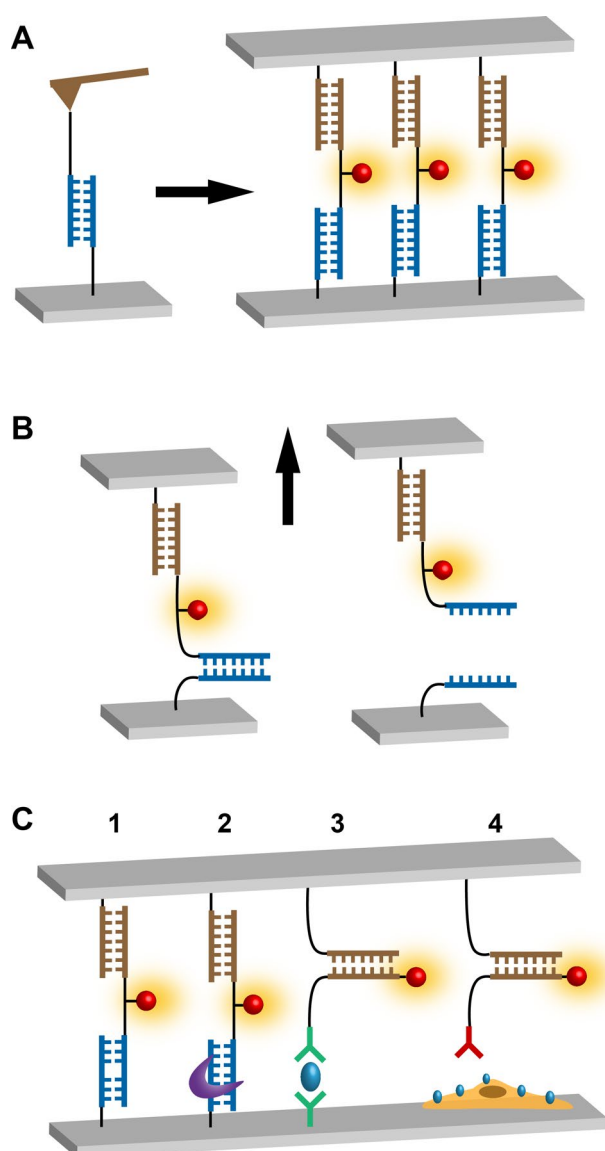


Figure 4. Implementation and application of the differential force assay. (A) Basic principle of the differential force assay. A macroscopic force probe, here the AFM cantilever, is replaced with a short double-stranded DNA (dsDNA) molecule that acts as a molecular force sensor (MFS). The MFS approach allows for testing many individual molecular interactions simultaneously. (B) One-to-one comparison of different pulling geometries of identical dsDNA sequences. A direct comparison of dsDNA loaded in shear and unzip geometry provides proof that the pulling geometry determines the rupture force of thermodynamically equally stable molecules. (C) Applications of the molecular force assay. DNA-based MFSs have been used for specifically detecting single mismatches (1) as well as a number of different DNA modifications, including the binding of proteins to dsDNA and dsRNA (2). Modifications of the assay have further been used for increasing the specificity of immunoassays (3) and for ‘stamping’ cells with ligands (4).

In a very first proof-of-principle experiment, two dsDNA molecules possessing the same sequence were compared with each other, applying force to one dsDNA molecule in the shear geometry while the other molecule was loaded in the unzip geometry (**Figure 4B**). When separating the two surfaces, it was observed that the dsDNA molecule loaded in the unzip geometry broke with a significantly higher probability, proving that the dissociation of two thermodynamically identical dsDNA molecule is indeed determined by the applied force. To test the force resolution of the newly developed assay, the same dsDNA sequence (perfect match; PM) was subsequently compared to a sequence with one single base-pair mismatch (MM), applying force to both dsDNA molecules in the shear geometry (**Figure 4C-1**). The different rupture probabilities of the two dsDNA molecules under investigation were clearly resolved as a result of this direct comparison of their mechanical stabilities. Such small differences can usually not be resolved using AFM-based SMFS, as they lie within the force resolution of the measurement.^[79]

In addition to the detection of single base-pair mismatches, this sensitive method was then successfully applied for the detection of other small modifications of the DNA sequence such as methylation^[89] and hydroxymethylation.^[90] The DFA method is further applicable for measuring DNA-ligand binding (**Figure 4C-2**) in crowded and complex molecular environments with a broad affinity range from picomolar (pM) to millimolar (mM).^[91-94] For example, it has been used for detecting the interaction and activity of different ligands and binding partners such as small molecules,^[91,95] polyamides,^[92,94,96] transcription factors^[97] and nucleases,^[93-95,98] with DNA, as well as with RNA.^[95] To provide the density needed for high-throughput applications, the system was further improved by using a miniaturization strategy^[93,94] or combining the DFA with a microfluidic chip.^[98]

DNA-based MFSs have not only been used for the detection of a number of different DNA modifications and interactions. The parallelization capacity of the DFA was further applied for the characterization of protein-protein interactions, especially antibody-antigen interactions.^[78,99-102] In particular, using a dsDNA molecule loaded in the unzip geometry, this MFS was used to implement a force-based sandwich immunoassay in a double-chip format (**Figure 4C-3**).^[78,99-101] One chip (the glass surface) contained specific capture antibodies to bind the antigen from solution. The second chip (the PDMS surface) carried the corresponding detection antibodies attached *via* the MFS. Upon contact of the two surfaces, the detection antibody specifically bound to its antigen and remained bound at this position when the two surfaces were separated. With this strategy, the detection antibodies were ‘stamped’ onto the antigen-containing surface only locally, utilizing the second chip. As no detection antibodies were freely diffusing in solution, non-specific binding was prevented. In addition, the attachment of the detection antibodies to the second chip *via* the MFS introduces a force threshold that can potentially be tuned to discriminate a specific antibody-antigen interaction from non-specific binding. The high local concentration of detection antibodies is therefore considered to increase both the specificity and the sensitivity of the assay, which are critical parameters for multiplexed sandwich immunoassays. In addition, its compatibility with standard biochip formats allowed the use for diagnostic applications in a simple and straightforward manner. Lastly, the DFA has also been utilized as a live-cell method for screening the expression of cell-surface receptors and for determining the relative binding strengths between different cell-surface receptors and their ligands (**Figure 4C-4**).^[103] It

should be noted at this point that the DFA method only provides a relative comparison of binding strengths. A detection of absolute force values requires a mechanical calibration of the MFS with single-molecule force spectroscopy before it is used in the DFA. The rupture force of an unknown interaction can then either be estimated from the rupture probabilities^[104] or alternatively from comparing the unknown interaction with a series of sensors that possess different rupture forces (mechanical analogue-digital conversion).^[103]

In parallel to the development of the DFA, efforts have been undertaken to combine SMFS with single molecule fluorescence detection.^[66,105-107] With the goal of integrating optical tweezers measurements with a fluorescence readout, the force-induced dissociation of short, fluorescently labeled dsDNA molecules was investigated.^[105,106] Just as in the DFA principle, the tested dsDNA molecule dissociated into two-components so that its mechanical response could be tested only once. Using a FRET-labeled DNA hairpin, opening and closing is reversible and the conformation of the molecule can be read out continuously while reporting on the applied force.^[108] Even though no application of the investigated DNA molecules as MFSs was proposed initially, this work is a crucial contribution for the development of the field. It shows that a mechanical process can be sensitively read out optically in real time at the single-molecule level. It further introduces strategies for the integration of optical tweezers with single-molecule fluorescence detection, which has become a powerful technological platform for MFS calibration. As an alternative to the DNA hairpin, also other mechanosensitive modules have been equipped with a continuous optical readout, followed by a systematic investigation using a combination of magnetic tweezers and single-molecule fluorescence.^[107,109] Random coil polymers, such as ssDNA or polyethylene glycol, act as entropic springs and their mechanical extension can be followed using a FRET pair. The implementation of this type of MFS has, for example, been used for measuring the forces acting within DNA loops that consist of single stranded and double stranded segments. All together, these studies demonstrate the possibility of utilizing the mechanical response of individual molecules for the highly sensitive detection of mechanical processes in a large number of different applications. These early MFS prototypes have set the stage for the implementation of DNA-based MFSs that are now becoming more and more widely used for cell biology applications.

6. Molecular force sensors for investigating cellular mechanotransduction

Following these initial experiments using molecular force sensors (MFSs), many new MFS designs have been developed for applications in both materials science and biology.^[66] It is not our goal to provide a complete overview of all these designs, but rather to highlight the MFSs that have been used for investigating the mechanical aspects of cellular mechanotransduction. MFSs have been used on the extracellular side for investigating the interaction between transmembrane receptors (*e.g.* integrins) and their ligands as well as on the intracellular side for determining the forces acting on different FA components. In contrast to the experiments described above, the direction of the applied force is less defined when measuring cell-generated forces, which can act parallel or perpendicular to the cell surface. As directional information is not available, the term molecular tension sensor is now frequently used for cellular applications.^[110-112] It should be noted, however, that the direction of the force acting on the sensor itself is not altered. The sensor will always align in the

direction of the applied force and its response mechanism is not affected. For consistency throughout the manuscript the term molecular force sensor (MFS) is still used whenever the focus is on mechanistic aspects and directional information is not of primary importance.

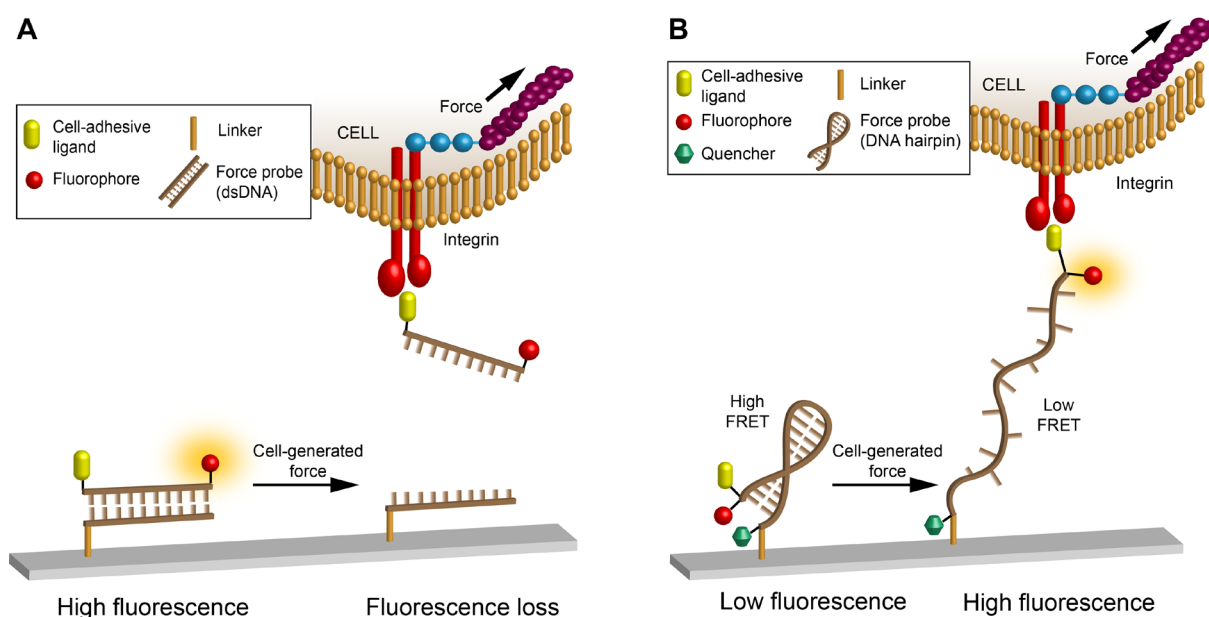


Figure 5. Design principles of molecular force sensors (MFSs). (A) Two-component MFS utilizing dsDNA oligonucleotides. One oligonucleotide is coupled to the substrate and the second oligonucleotide is functionalized with a cell-binding ligand (*e.g.* a RGD peptide). The DNA duplex ruptures when the cells apply sufficient force *via* their cell-surface receptors (*e.g.* integrins). The oligonucleotide that carries the cell-binding ligand is further labeled with a fluorophore. Cell-generated forces break the DNA duplex, leading to the detachment of the cells together with the fluorescently labeled probe and, consequently, a loss of fluorescence from the substrate. (B) One-component MFS utilizing a mechanoresponsive module (*e.g.* a DNA hairpin). The hairpin is functionalized with one fluorophore and a quencher that undergo Förster Resonance Energy Transfer (FRET). When sufficient force is applied, the DNA hairpin opens, leading to a change in the FRET efficiency and, consequently, an increase in donor fluorescence.

Current sensor designs can be divided into two categories: (i) two-component MFSs that utilize the same detection principle as the DNA duplexes described above, *i.e.* these MFSs break once the applied force exceeds a threshold value (**Figure 5A**). (ii) one-component MFSs that utilize a mechanoresponsive module, such as a DNA hairpin or a polymeric entropic spring. This module is inserted into a chain of molecules under tension where it acts as a spring and reports on the force acting along the chain (**Figure 5B**). To date, two-component MFSs have only been used on the extracellular side, whereas one-component MFSs have been employed both intra- and extracellularly.

6.1 Two-component sensors for extracellular force measurements

Extracellular MFS designs are generally equipped with a cell-binding ligand to allow for the specific interaction of cells with the MFSs. At the same time, the MFSs are immobilized on a substrate surface (**Figure 5**). When cells are seeded on top of a MFS-functionalized surface,

cell surface receptors start to engage with the cell-binding ligands and, consequently, the cells start to apply traction forces on the MFSs. In the case of a two-component MFS, the sensor breaks once the applied force exceeds the stability limit of the MFS (**Figure 5A**). If cells are able to generate forces larger than the mechanical stability of the MFS, they disintegrate the MFS and cannot attach to the surface. In contrast, cells are able to mechanically interact with the surface when the mechanical stability of the MFS is sufficiently high, allowing cells to adhere and grow. Using this experimental strategy consequently allows for directly testing the threshold force required for cell attachment.

In a first proof-of-principle experiment by Ha and coworkers, dsDNA-based MFSs were used to determine the threshold force required for the attachment of $\alpha_v\beta_3$ integrins to cRGDFK ligands. Making use of the fact that the rupture force of dsDNA depends on the pulling geometry (shear vs. unzip; **Figure 4B**),^[78] a set of 9 different MFSs, termed ‘tension gauge tethers’ (TGTs), was designed. The TGT sensors break at different forces in the range from ~12-56 pN.^[112] The pulling geometry was determined by simply attaching the dsDNA molecule to the substrate at different positions. The estimated threshold force for anchoring the TGT in the unzip geometry was ~12 pN, while it was about ~56 pN in the shear geometry (force predicted at which 50 % of dsDNA molecules rupture when mechanically loaded for 2 seconds^[83,112,113]). Intermediate attachment positions yielded additional rupture forces to cover the range between these two extremes. Using CHO-K1 cells and 3T3 fibroblasts, it was shown that cells are only able to adhere to the substrate if the mechanical stability of the TGT was at least ~40 pN. This threshold value was later confirmed with a number of other non-cancerous as well as cancerous cell lines.^[114]

In this first experiment, cell growth was the only readout parameter used to monitor the interaction of the cells with the TGTs. In later experiments, this sensor design was equipped with a fluorescent readout (**Figure 5A**).^[115,116] A fluorophore was coupled to the sensor component that carries the cell-binding ligand. Upon rupture of the TGTs, this component detached from the surface, leading to a loss of the fluorescence signal at the positions where the cells interacted with the TGTs. It was observed that TGTs with a low mechanical stability (<40 pN) were ruptured everywhere on the surface. Cells continuously pull on these TGTs and cannot attach, as the TGTs do not provide the possibility for forming stable focal adhesions. In contrast, rupture was mostly observed in designated areas when using the TGT with a predicted stability of 56 pN. These areas were correlated with the positions of FAs and stress fibers, suggesting that their formation requires at least 56 pN of tension across integrin–ligand bonds.^[115] Interestingly, a homogeneous loss of the fluorescence signal was detected for the TGT with a predicted stability of 43 pN where cell attachment was already seen. Under these conditions no FAs and stress fibers formed, however, suggesting that this force represents the integrin–ligand force for the initial stages of cell attachment. This experiment was then further refined using a mixture of two fluorescently labeled TGTs that rupture at different forces (12 pN and 56 pN, respectively).^[116] While cells did not attach to a surface functionalized only with the ‘low force’ TGT, they were able to do so if a very small amount of the ‘high force’ TGT was co-immobilized on the surface. Most likely 1-2 ‘high force’ TGT molecules per cell are sufficient to facilitate cell attachment, indicating that cells are extremely sensitive when detecting the mechanical properties of their surroundings.

The developed set of two-component MFSs represents a highly versatile toolbox for measuring tension acting between cell-surface receptors and their ligands. Additional experiments have been performed to characterize the mechanics of the Notch receptor,^[112,117] the B-cell^[118] and T-cell receptors^[119] as well as E-cadherin and P-Selectin.^[120] At the same time, these TGT sensors can also be used for studying mechanotransduction mechanisms. It is still a matter of debate how global material properties (such as stiffness) and local mechanical stimuli (such as locally acting forces) contribute to the regulation of cell behavior.^[11,121,122] Two-component MFSs limit the maximum force that is applied to a single cell-surface receptor and, consequently, allow for dissecting these different contributions. Moreover, also the nature of the linkage between the substrate and the cell-binding ligand can be varied. In a series of elegant experiments, the TGTs were immobilized on a solid glass surface *via* PEG spacers of different length.^[114] Alternatively, the TGTs were attached to polyacrylamide^[114] or alginate gels^[123] of different stiffness. Even though no unambiguous answer could be obtained, the results of these experiments suggest the involvement of both global and local factors for determining cellular behavior.

6.2 One-component sensors for extracellular force measurements

The prototype examples described in section 5^[107-109] inspired the subsequent development of one-component MFSs for cell biology applications. The key feature of these one-component MFS designs is a mechanosensitive module that responds to an applied force in a well-defined way (**Figure 5B**). For extracellular force measurements the mechanosensitive module is functionalized with a cell-binding ligand and a functional group that allows for its immobilization to the substrate surface. The module is further equipped with two chromophores forming a FRET pair. In this design, the FRET efficiency is a sensitive reporter of the mechanically induced elongation of the mechanosensitive module and, consequently, of the applied force.

Table 2. Technical properties of one-component MFSs used for extracellular force measurements

Sensor	Mechanism	Force Range	Sensor Calibration	Signal	Readout	Reference(s)
PEG _n	entropic spring	~1-30 pN	Calculated from WLC model	FRET	analog (continuous)	[111,124,125]
PEG _n	entropic spring	~1-30 pN	Calculated from WLC model	NSET	analog (continuous)	[126,127]
flagelliform (GPGGA) ₈	linear spring	~1-7 pN	SMFS (optical tweezers)	FRET	analog (continuous)	[31,110,128]
DNA hairpin	unfolding	~6-17 pN	SMFS (optical tweezers)	FRET	digital (ON-OFF)	[129]
DNA hairpin	unfolding	~5-16 pN	SMFS (BFP)	FRET	digital (ON-OFF)	[119,130]
titin	unfolding	~80-200 pN	SMFS (AFM)	NSET	kinetic	[131]

FRET: Förster resonance energy transfer; NSET: nanometal surface energy transfer; WLC: worm-like chain; BFP: bio-membrane force probe; AFM: atomic force microscope

To date, different mechanosensitive modules have been used, employing synthetic polymers, DNA hairpins or peptide and protein structures (**Table 2**). Synthetic polymers such as polyethylene glycol (PEG) are powerful mechanosensitive building blocks as they are mechanically well-characterized. Their force *vs.* extension characteristics can be described with known polymer models, such as the worm-like chain (WLC) or freely-jointed chain (FJC) models. The force *vs.* extension relationship allows for directly correlating the FRET efficiency with the force acting on the MFS.^[111,124-127] Using the extensible WLC model for PEG (and considering the Förster radius of the FRET pair), a dynamic force range between 1-30 pN is expected depending on the length of the PEG building block (PEG₁₂-PEG₈₀).^[111,124,127]

In a first proof-of-principle experiment by Salaita and coworkers, the PEG building block was functionalized with epidermal growth factor (EGF) to determine the forces involved in the internalization of the EGF receptor.^[111] The EGF-functionalized PEG chain was further equipped with a donor-quencher pair and immobilized to a glass surface using the streptavidin–biotin interaction. When growing cells on top of the resulting tension sensor-functionalized surface, a threshold of 4 pN was detected for the EGF–receptor interaction. The same design was later used in a series of other experiments to determine the forces acting between $\alpha_v\beta_3$ integrins and several integrin ligands, including the cRGDfK peptide.^[124-127] Following the fluorescence intensity over extended periods of time, revealed that tension acting across one single integrin bond can dissociate the streptavidin–biotin interaction that was used for tethering the sensor to the surface.^[124] This result clearly suggests that integrin–ligand interactions can withstand extremely high forces, a result that is consistent with those obtained with the two-component dsDNA-based sensors described above and from SCFS and SMFS experiments.^[120] These results highlight that non-covalent interactions should be avoided when immobilizing MFSs to the substrate.

To overcome this stability problem, a new immobilization method was implemented. PEG-based sensors carrying a terminal thiol group were attached to gold nanoparticles (AuNPs) deposited on a surface.^[126,127] Utilizing AuNPs did not only provide a more robust immobilization method, but also eliminated the need for a FRET acceptor. Donor fluorescence is quenched *via* nanometal surface energy transfer (NSET), providing better signal-to-noise ratios and a larger distance range for energy transfer. Initial experiments with this improved design yielded only average integrin–ligand forces of ~ 1 pN, contradicting the above results.^[126] The system further allowed for investigating the effect of ligand spacing by adjusting the distance between AuNPs in the array.^[127] These results have shown that a large ligand spacing (100 nm) prevents the formation of FAs and stress fibers and that the integrin–ligand forces do not exceed 3 pN. In contrast, FAs are formed if the ligand spacing is 50 nm and the forces reach up to values of 6-12 pN. Again, comparably low forces were detected even though the previously described increase following FA and stress fiber formation was also observed in this experiment.^[116] One possible explanation for these discrepancies is that the number of MFSs that are mechanically coupled to an integrin receptor is not known. The fluorescence signal, however, is obtained from the ensemble of all available (mechanically coupled and non-coupled) sensor molecules. Alternatively, the force distribution across different integrin–ligand bonds may be heterogeneous in space and time. Only a small number

of integrins may be able to apply high forces that lead to the observed rupture of strong non-covalent bonds.^[116]

With the PEG-based sensor design it is not possible to test this hypothesis as the continuous (analog) ensemble readout averages over a large number of integrin–ligand interactions in the optical detection volume. To address this issue, FRET-labeled tension sensors were diluted with non-labeled sensors with the goal of observing the FRET-labeled sensors with single-molecule resolution.^[128] For this experiment a (GPGGA)₈ peptide, derived from the spider silk protein flagelliform,^[110] was used as the mechanosensitive module (described in more detail in **section 6.3**). Again, forces ranging from 1-5 pN were observed with this system. This result strongly suggests that the majority of sensors are indeed only loaded with forces of maximally 5 pN and that high force events are so rare that they could not be identified.

Another solution to the ensemble averaging problem may be the use of digital one-component MFSs that possess only one ON (high FRET) and one OFF (low FRET) state. Using this strategy, the relative fraction of sensors in either state can be directly calculated from the FRET efficiency of the ensemble. DNA hairpins fulfill all criteria of digital MFSs.^[129,130] Provided that the hairpin is short enough, it unfolds cooperatively when mechanically stretched,^[132] thereby providing a force threshold that can be tuned in a sequence dependent manner (~5-16 pN; corresponding to the force where 50 % of the hairpins are unfolded in a force clamp experiment). Quantitative imaging with these sensors revealed that the integrin–ligand forces were highly dynamic and heterogeneous and that a significant number of integrin–ligand forces exceeded the force threshold of the sensor. Due to the limited force range of the hairpins, the highest possible integrin–ligand forces could not be determined, however. Subsequently, a digital one-component MFS based on the mechanically well-characterized protein titin was developed.^[131] Titin unfolds at forces from ~150-300 pN (determined from AFM-based single-molecule force spectroscopy at different pulling speeds ranging from ~0.01-10 $\mu\text{m/s}$ ^[133,134]), thereby covering the high force range. Titin unfolding observed in this experiment confirmed the previous results that integrins are indeed able to apply high forces.

Even though the currently available results obtained from extracellular sensors appear partially inconsistent, a number of conclusions can be drawn that link all observations together. Ensemble and time-averaged forces from MFSs and a number of other experiments yield integrin–ligand forces ranging from <1 pN up to ~10 pN.^[3] This does not exclude, however, that a small number of integrins in the population can experience much higher forces and that the forces experienced may vary over time. One next step is clearly to investigate these heterogeneities and to unravel the functional relevance of these high force interactions. It should be noted here, that discrepancies between the absolute force values determined with different MFSs may also originate from different calibration methods and the lack of knowledge of the cell-applied loading rate. A more detailed discussion of these practical limitations is given in section 7.

6.3. One-component sensors for intracellular force measurements

The forces acting on the extracellular side propagate intracellularly, where they distribute across FA proteins and the cytoskeleton. Understanding intracellular force transduction requires MFSs that can be integrated into these ‘host’ protein structures as a ‘guest’ without

disturbing their biological function. For this purpose, genetically encoded MFSs have been developed, where a mechanosensitive module is inserted into a protein of interest. Just as for the one-component sensors used extracellularly, the mechanosensitive building block is again equipped with a fluorescent reporter system that converts molecular forces into optical signals. In contrast to extracellular MFSs, fluorescent proteins are used that are encoded as a fusion protein together with the MFSs.

Table 3. Technical properties of one-component MFSs used for intracellular force measurements

Sensor	Mechanism	Force Range	Sensor Calibration	Signal	Readout	Reference(s)
α -helix	extension or unfolding	unknown	DNA spring	dFRET	analog (continuous)	[135,136]
GFP-cpGFP	physical interaction	unknown	none	PRIM	digital (ON-OFF)	[137,138]
flagelliform (GPGGA) _n	linear spring	~1-6 pN	SMFS (optical tweezers)	dFRET	analog (continuous)	[110]
spectrin	extension or unfolding	unknown	DNA spring	dFRET	unknown	[139]
FP pair	reorientation	unknown	DNA spring	oFRET	analog (continuous)	[140]
villin headpiece	unfolding	~1-10 pN	SMFS (optical tweezers)	dFRET	analog (continuous)	[141]

FP: fluorescent protein; cpGFP: circularly permuted green fluorescent protein; dFRET: distance-dependent Förster resonance energy transfer; oFRET: orientation-dependent Förster resonance energy transfer; PRIM: proximity imaging

To date, three different strategies have been employed to generate the optical readout signal (Table 3). The most frequently used strategy is distance-dependent FRET (dFRET) between two fluorescent proteins, in the same way as for extracellular one-component MFSs.^[110,135,141,142] The FRET efficiency can further be modulated by mechanically-induced changes in the orientation of two chromophores (oFRET) and this principle has also been implemented for MFS design.^[140] Lastly, two fluorescent proteins can physically interact by dimerization, thereby changing their spectral properties; a phenomenon utilized in proximity imaging (PRIM). When mechanically stretched, the two fluorescent proteins dissociate and the fluorescent properties match those of the monomer.^[137,138] In the following, we will only focus on MFSs that utilize the dFRET strategy, as the other sensors have not been utilized for investigating mechanotransduction mechanisms, but rather cytoskeletal forces generated by other cellular processes.

Focusing on the dFRET strategy, the first example of an intracellular one-component MFS for the live-cell imaging of intracellular forces was created by Sachs and coworkers.^[135] A stable α -helix was equipped with a N-terminal and a C-terminal fluorescent protein and inserted into a number of different proteins such as α -actinin, spectrin and filamin A.^[135] Using this MFS, it was shown qualitatively that the FRET efficiency of the MFS changes at the leading and trailing edge when cells move. An attempt was made to calibrate the applied force vs. the FRET efficiency, using a so-called DNA spring.^[143] The dynamic force range was estimated

to span the range up to $\sim 5\text{-}7$ pN.^[136] This can only be considered as a semi-quantitative calibration, however, as a large number of assumptions have been made when calculating the equilibrium force that is applied by the DNA spring.

With the goal of creating a MFS that matches the compliance of the host protein, the α -helix was later replaced by a spectrin repeat, composed of three folded α -helices.^[139] The force response of the new MFS was again estimated using the DNA spring and the MFS was shown to be sensitive in a range up to $\sim 5\text{-}7$ pN. Using AFM-based SMFS, however, spectrin was recently shown to unfold at forces between 20-40 pN.^[144] Inserted into the FA protein α -actinin, it was subsequently used for investigating the mechanical stress across this protein at FA sites when cells were exposed to osmotic stress^[139] or shear stress^[142,145] and when grown on micropatterned surfaces.^[146] Most interestingly, the sensor was used for investigating possible tension across α -actinin during FA growth.^[147] It was shown that α -actinin is indeed involved in force transduction between integrins and actin. In fact, the force acting on α -actinin increased during FA growth, suggesting that α -actinin is involved in the regulation of FA size.

The first fully calibrated MFS developed for intracellular applications was introduced by Grashoff and coworkers.^[110] The mechanosensitive building block consisted of the 40 amino acid long sequence (GPGGA)₈ derived from the spider silk protein flagelliform. Again, the MFS module was inserted between two different fluorescent proteins, forming a FRET pair. As the mechanical response of the peptide sequence was initially unknown, it was calibrated using an optical tweezers setup combined with single-molecule fluorescence detection. In this way, a direct correlation between the applied force and the resulting FRET efficiency could be established. During cyclic stretching with the optical tweezers the peptide showed a reversible response with a dynamic force range of $\sim 1\text{-}6$ pN^[110] and a linear force extension curve.^[148] The MFS, also called ‘tension sensor module’ (TSMoD), was inserted into the FA protein vinculin and the average force acting on vinculin was determined to be ~ 2.5 pN. Interestingly, this force lies in the same range as the average force that has been determined for integrin–ligand interactions on the extracellular side as determined with extracellular one-component MFSs.^[126-128] It was further observed that this force varied within a certain range between different FAs.

Having established the functionality of TSMoD and having confirmed that it does not alter wildtype function,^[19,21,110] it was subsequently used for investigating the force distribution across vinculin in more detail. For example, femtosecond laser nanosurgery was employed to cut individual stress fibers and to follow the subsequent redistribution of the mechanical load at different FAs.^[149] It was shown that tension is not redistributed across FAs homogeneously, but that some FAs (*i.e.* vinculin molecules) feel higher tension, while it decreases on others. In a more detailed study, the size of FAs was followed over time while also measuring the tension on vinculin.^[150] This experiment also confirmed that the FA population is heterogeneous. For the majority of FAs an increased vinculin tension was correlated with FA growth, however, other FAs were identified where FA growth and vinculin tension were negatively correlated. Interestingly, medium sized FAs showed a positive correlation, while a negative correlation was determined for both small and large FAs. This result clearly shows that tension acting across vinculin is highly dependent on the functional state of the FA.

Since its introduction, TSMoD has not only been used for studying tension across vinculin. It has also been inserted into a large number of other proteins that are considered to experience mechanical forces, such as E-cadherin,^[151,152] VE-cadherin,^[153] PECAM,^[153] spectrin^[154,155] and MUC-1.^[156] While it has mostly been applied in cell culture experiments, it has also already been used in living organisms such as *C. elegans*.^[154,155]

One crucial limitation of TSMoD is its very small force range between 1-6 pN. Considering the wide distribution of forces detected extracellularly, clearly new MFSs with an extended force range are required for intracellular applications. A new MFS design, based on the villin headpiece peptide (HP35), was introduced recently and calibrated using optical tweezers.^[141] For calibration, the equilibrium force was determined where 50 % of the peptide is unfolded. For the wildtype peptide a force of 7.4 pN was determined, indicating that its dynamic range is shifted to higher forces, when compared to TSMoD. In addition, a stabilized mutant (HP35st) was tested and found to unfold at an equilibrium force of 10.6 pN. The new sensors were then used for measuring tension acting on the key FA protein talin. It was inserted between the unstructured linker region connecting the head and rod domains of mouse talin-1 and talin-2. It was shown that talin is mechanically loaded with an average tension of 7-10 pN, again showing agreement with the average forces detected for integrin–ligand interactions. Overall, intracellular one-component MFSs have been used for measuring forces acting on three crucial FA proteins, namely α -actinin, vinculin and talin. For vinculin and talin, where a calibrated MFS has been used, the forces maximally reach up to 10 pN. These forces match the average forces that have been determined for integrin–ligand interactions on the extracellular side. It is currently not clear, if intracellular forces can also reach up to much higher values as no MFSs are currently available to detect forces above 10 pN. Considering that a heterogeneous force distribution has already been observed for the FA protein vinculin, it appears likely that the molecular forces acting on the intracellular side are equally broad. Even though the average forces at the intra- and extracellular sides seem to match, these results should still be interpreted with care as the stoichiometry between different FA proteins is not clear in many cases, *e.g.* talin can bind many molecules of vinculin in its activated state.^[33]

7. General considerations for the design and application of molecular force sensors

In recent years many different MFS designs have been introduced for biological applications, mostly in the area of cell biology. They have clearly evolved into powerful tools for studying molecular mechanisms and novel information about FA mechanics has been obtained. Even though several general principles – including functional, spatial and temporal FA heterogeneities – have been established, the measurement of absolute force values has remained a challenge. In many cases, the dynamic range of the MFS is rather small and MFSs have either not been calibrated or different methods were used for their calibration.

7.1 Force range and MFS calibration

A large diversity of different building blocks has been used for the design of MFSs. The majority of MFSs, however, can only report on forces up to maximally ~60 pN. The only exception is the recently introduced titin-based MFS (150-300 pN).^[131,133,134] No MFS design is currently available that fills the gap or even spans the complete force range accessible to

biological systems. Extending the force range of a certain MFS design is also not an easy task. The rupture force of dsDNA-based force sensors, for example, plateaus at a force of ~ 65 pN where the DNA molecule undergoes an unfolding transition (B-S transition).^[86,87] Increasing the rupture force above this value is not possible when using the 4 natural bases A, T, C and G, but may be achieved when using a peptide nucleic acid (PNA) backbone^[157,158] or when substituting individual pyrimidine bases with their propynyl derivatives.^[102] All currently used intracellular MFSs employ fluorescent proteins for the FRET readout. The MFSs are designed such that the force travels through the fluorescent proteins. This is not a problem for MFSs that are responsive in the low force range, where the fluorescent proteins are mechanically stable.^[141] Mechanically induced unfolding of the β -barrel structure fluorescent proteins occurs at forces >80 pN,^[131,144,159] however, so that new fluorescent labeling strategies using organic fluorophores will be required for these experiments.

The next step following MFS design is to calibrate its mechanical response and to correlate it to the fluorescence signal. In many cases an accurate calibration has not yet been obtained. Some MFS building blocks are mechanically well-characterized, such as PEG and dsDNA. PEG is usually described with the worm-like chain (WLC) model, allowing for a straightforward calculation of its force extension behavior. In this case a straightforward calibration of the optical signal (change in FRET efficiency) vs. the applied force can be achieved. Also for dsDNA oligonucleotides loaded in the shear geometry a model has been proposed by De Gennes,^[113] treating dsDNA as a 2-dimensional ladder. The model predictions have later been experimentally verified with a force clamp magnetic tweezers experiment.^[83] Using this model, the mechanical stability of the two-component dsDNA-based MFSs (*i.e.* the TGTs) was calculated.^[112] Recently, a more accurate 3D model was developed, however.^[160] The improved model confirms the rupture forces calculated for the pure shear and unzip geometries, but yields significantly lower forces for the intermediate geometries. These discrepancies show that an experimental calibration should be performed even for mechanically well-characterized molecules. A calibration is absolutely essential for mechanical building blocks with an unknown mechanical response, such as the flagelliform^[110] or villin headpiece peptides.^[141] To do so, an integrated single-molecule force-fluorescence setup was used,^[110] which is clearly the best strategy to obtain the calibration.^[66,105-107]

Even though efforts have been made in many cases to obtain at least a semi-quantitative calibration, it needs to be considered that the force values given have been determined with different methods. For the previously mentioned dsDNA oligonucleotides the calculated mechanical stability represents the minimum force that needs to be applied to rupture the dsDNA molecule within 2 seconds,^[83,112] whereas the forces given for flagelliform,^[110,148] HP35/HP35st^[141] and the DNA hairpin sensors^[129,130] represent the equilibrium force, where 50 % of the MFS molecules are in the unfolded/extended state (measured in force clamp optical tweezers experiments). Considering these different calibration methods, it is most likely not possible to directly compare the obtained force values.

7.2 Stability and kinetics of bonds under force

When performing the calibration, it needs to be considered that force is not an intrinsic property of a molecule or a molecular interaction. It does not only depend on the free energy

ΔG of the molecular process (**Figure 6**), but also on the temperature T and the rate of force application (*i.e.* the loading rate). According to Bell's model^[161] the energy barrier ΔG is lowered by the applied force F (Eq. 1), thereby speeding up the process under investigation (*e.g.* bond dissociation).

$$k(F) = \nu \cdot e^{-\frac{(\Delta G - F \cdot \Delta x)}{k_B T}} \quad (1)$$

with $k(F)$ being the rate of the mechanically accelerated reaction, ν the attempt frequency, Δx the distance between the ground and the transition state (*i.e.* the potential width) and k_B the Boltzmann constant.

As barrier crossing is a thermally assisted process, bond rupture generally depends on the loading rate $r = dF/dt$ as described in detail by Evans.^[162,163] According to the frequently used Bell-Evans model, the force F depends on the loading rate as described in Eq. 2.

$$F(r) = \frac{k_B T}{\Delta x} \cdot \ln \left(\frac{r}{k_0} \cdot \frac{\Delta x}{k_B T} \right) \quad (2)$$

with k_0 representing the rate of the reaction at zero force.

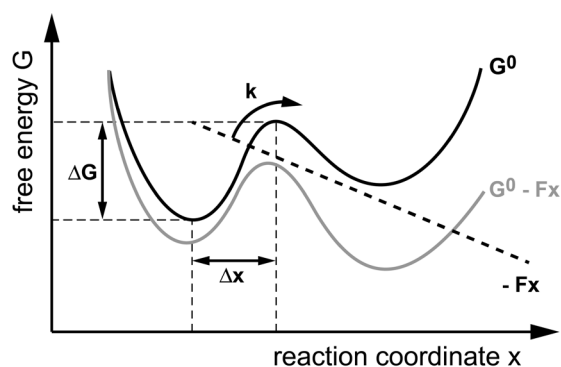


Figure 6. Effect of force on the free energy landscape of a molecular process. Assuming a simple two-state system, the applied force F lowers the energy barrier ΔG of the reaction by the amount $-Fx$ so that the molecular process is accelerated.

When calibrating a MFS, it is consequently important to consider the real biological situation, in particular the loading rate (and the temperature). The loading rate, which acts at individual integrins in focal adhesions, is not known. It may further dynamically change over time and also the timescale that the molecules are subjected to load may vary. The loading rate is difficult to measure directly and Sheetz and coworkers have provided an estimate of 0.007-4 pN/s.^[3] This range is large and far below the loading rate range usually applied in SMFS. One strategy to avoid these complications with MFS calibration is to use MFSs that do not show any or only a very weak loading rate dependence. This is the case when the mechanically induced reaction is reversible on the experimentally accessible timescale, *i.e.* when the backward rate is faster than the rate of force application. Such quasi-equilibrium processes are frequently observed for reactions that occur at low forces where many small molecular rearrangements occur sequentially. This includes the mechanical extension of polymers, such as PEG, as well as the unzipping of dsDNA.^[88] It may equally be the case for the stretching of the flagelliform^[110] and villin headpiece^[141] peptides.

Processes that occur at higher forces do usually involve high-energy barriers so that the reaction is not reversible on the experimental timescale. In fact, most mechanically induced processes show a strong loading rate dependence. Considering that the loading rates in the biological systems are very low, one may assume a constantly applied force acting on the MFS. As an approximation, it may therefore be sufficient to determine the force where 50 % of the MFSs become active in a force clamp experiment, as it has been done for the dsDNA-based MFSs^[112,129] as well as for the flagelliform^[110] and villin headpiece^[141] peptides. For an unknown, newly developed MFSs a full calibration at different loading rates is recommended, however, as this allows for the extraction of the full set of parameters that describe the MFSs (see Eq. 2), *i.e.* the rate of the process at zero force (k_0) and the potential width (Δx). For a fully calibrated system, the rupture force can then be calculated for any loading rate and temperature relevant for the biological system under investigation. Once these parameters are available, also the lifetime of individual MFSs can be used to extract the force, instead of the fraction of MFSs that have been activated. This strategy has recently been implemented using a disulfide locked titin domain as an MFS where the lifetime of the disulfide bond was used to obtain information about the applied force acting on the molecule.^[131]

Considering the above limitations in the MFS force range and the lack of knowledge of the loading rate in biological systems, variations in the absolute force values appear very likely. Even though the results obtained seem to provide a consistent picture of the forces acting at FAs, it cannot be fully ruled out that the variations in the measured forces are simply the result of MFS calibration errors. At the current stage, a new fully calibrated MFS design is urgently needed that spans the complete force range from 2-200 pN. This new design will allow for a more detailed investigation of spatial and temporal heterogeneities in the forces that act across single integrins.

8. Summary and perspectives

The quickly developing field of molecular force sensors (MFSs) is continuously providing new tools for investigating the molecular mechanisms of cellular mechanotransduction, with a special focus on mechanical processes at focal adhesions (FAs). Current results suggest that the forces acting at FA sites span a large range, and that they are heterogeneous in space and time. Even though this seems to emerge as a general principle, calibration errors of the MFSs may contribute to the variations in the absolute force values detected. One may argue that the knowledge of absolute force values may not be essential for mechanistic studies; however, they will be essential for the comparison of results. It is therefore crucial for the further development of the field to calibrate the MFSs and to gain more insight into the loading rates acting at FA sites. Also, new MFSs will have to be developed that span a larger force range so that the complete range of forces can be measured in one and the same experiment. Especially for intracellularly used MFSs this will be a challenging task, as the MFSs must not interfere with the function of the host protein and new readout strategies will have to be implemented. When developing new MFSs for the extracellular side, protein building blocks are preferred. DNA does not naturally exist in the extracellular microenvironment. Introducing foreign DNA to cells might affect the cellular response in an ambiguous way and the results may conflict with the usual behavior of cells within their natural ECM.

Apart from these limitations, most currently available MFSs have been designed for investigating cell-ECM interactions in two-dimensional (2D) cell culture assays using solid substrates, most commonly glass surfaces with an elastic modulus reaching up to gigapascal (GPa) values. In natural tissues, cells experience a three-dimensional (3D) environment with different stiffness values (*e.g.* $E_{\text{brain}} \sim 1$ kPa, $E_{\text{muscle}} \sim 10$ kPa, $E_{\text{collagenous bone}} \sim 100$ kPa^[11]). Clearly, as an ultimate goal, the power of MFSs needs to be combined with the materials science point of view. This crucial next step towards the development of 3D platforms will allow for investigating molecular force transduction in an environment that mimics the natural ECM more closely.

The toolkit of MFSs allows for a large number of interesting combinations with other techniques used for studying mechanotransduction. One obvious combination is with traction force microscopy where it will allow for correlating the average force on a given area with molecular information. The combination with TFM will further add directionality information that is missing when using MFSs alone. Also, integrating MFS detection with 2D and 3D micro- and nano-structures will provide new insights into the interplay between geometrical and mechanical effects on cellular behavior.^[127] Clearly, MFSs are not only simple measurement tools. Two-component MFSs define a threshold force that is maximally felt by a specific interaction. They can therefore also be used for triggering cells with a defined mechanical stimulus and for influencing cellular behavior. Two-component MFSs may further be utilized as reversible mechanosensitive material crosslinkers^[164] and thereby provide currently inaccessible information about the mechanical interaction between cells and materials in a 3D context. Combined with proteomic analyses, the effect of the mechanical stimulus on cellular mechanotransduction pathways can be investigated. To conclude, MFSs have emerged as powerful tools for a large number of different applications. Considering that the field is still in its early stages, many new exiting MFS designs and areas of application are expected to appear in the near future.

Acknowledgements

The authors thank Ruby M. A. Sullan for inspiring discussions as well as Patricia Lopez Garcia and Roel Hammink for critically reading the manuscript. This work was supported by the Max Planck Research School (IMPRS) on Multiscale Bio-Systems and the Max Planck Society.

References

- [1] Y. F. Dufrene, E. Evans, A. Engel, J. Helenius, H. E. Gaub, D. J. Müller, *Nat. Methods* **2011**, *8*, 123.
- [2] A. E. X. Brown, D. E. Discher, *Curr. Biol.* **2009**, *19*, R781.
- [3] S. W. Moore, P. Roca-Cusachs, M. P. Sheetz, *Dev. Cell* **2010**, *19*, 194.
- [4] I. Schoen, B. L. Pruitt, V. Vogel, *Annu. Rev. Mater. Res.* **2013**, *43*, 589.
- [5] N. Wang, J. Butler, D. Ingber, *Science* **1993**, *260*, 1124.
- [6] V. Vogel, *Annu. Rev. Biophys. Biomol. Struct.* **2006**, *35*, 459.
- [7] A. S. LaCroix, K. E. Rothenberg, B. D. Hoffman, *Annu. Rev. Biomed. Eng.* **2015**, *17*, 287.
- [8] E. A. Evans, D. A. Calderwood, *Science* **2007**, *316*, 1148.

- [9] M. P. Sheetz, D. P. Felsenfeld, C. G. Galbraith, *Trends Cell Biol.* **1998**, *8*, 51.
- [10] A. J. Garcia, M. a. D. Vega, D. Boettiger, *Mol. Biol. Cell* **1999**, *10*, 785.
- [11] A. J. Engler, S. Sen, H. L. Sweeney, D. E. Discher, *Cell* **2006**, *126*, 677.
- [12] M. J. Paszek, N. Zahir, K. R. Johnson, J. N. Lakins, G. I. Rozenberg, A. Gefen, C. A. Reinhart-King, S. S. Margulies, M. Dembo, D. Boettiger, D. A. Hammer, V. M. Weaver, *Cancer Cell* **2005**, *8*, 241.
- [13] E. M. Puchner, A. Alexandrovich, A. L. Kho, U. Hensen, L. V. Schäfer, B. Brandmeier, F. Gräter, H. Grubmüller, H. E. Gaub, M. Gautel, *Proc. Natl. Acad. Sci. U. S. A.* **2008**, *105*, 13385.
- [14] S. F. Heucke, E. M. Puchner, S. W. Stahl, A. W. Holleitner, H. E. Gaub, P. Tinnefeld, *Int. J. Nanotechnol.* **2013**, *10*, 607
- [15] X. Zhang, K. Halvorsen, C.-Z. Zhang, W. P. Wong, T. A. Springer, *Science* **2009**, *324*, 1330.
- [16] J. P. Müller, S. Mielke, A. Löff, T. Obser, C. Beer, L. K. Bruetzel, D. A. Pippig, W. Vanderlinden, J. Lipfert, R. Schneppenheim, M. Benoit, *Proc. Natl. Acad. Sci. U. S. A.* **2016**, *113*, 1208.
- [17] J. D. Humphries, N. R. Paul, M. J. Humphries, M. R. Morgan, *Trends Cell Biol.* **2015**, *25*, 388.
- [18] D. E. Jaalouk, J. Lammerding, *Nat. Rev. Mol. Cell Biol.* **2009**, *10*, 63.
- [19] A.-L. Cost, P. Ringer, A. Chrostek-Grashoff, C. Grashoff, *Cell. Mol. Bioeng.* **2015**, *8*, 96.
- [20] C. Jurchenko, K. S. Salaita, *Mol. Cell. Biol.* **2015**, *35*, 2570.
- [21] A. Freikamp, A. Mehlich, C. Klingner, C. Grashoff, *J. Struct. Biol.* **2016**, DOI: 10.1016/j.jsb.2016.03.011.
- [22] W. J. Polacheck, C. S. Chen, *Nat. Methods* **2016**, *13*, 415.
- [23] R. O. Hynes, *Cell* **2002**, *110*, 673.
- [24] B. Geiger, J. P. Spatz, A. D. Bershadsky, *Nat. Rev. Mol. Cell Biol.* **2009**, *10*, 21.
- [25] L. B. Case, C. M. Waterman, *Nat. Cell Biol.* **2015**, *17*, 955.
- [26] Y. Takada, X. Ye, S. Simon, *Genome Biol.* **2007**, *8*, 215.
- [27] M. Vicente-Manzanares, C. K. Choi, A. R. Horwitz, *J. Cell Sci.* **2009**, *122*, 199.
- [28] J. D. Humphries, A. Byron, M. J. Humphries, *J. Cell Sci.* **2006**, *119*, 3901.
- [29] M. Barczyk, S. Carracedo, D. Gullberg, *Cell Tissue Res.* **2010**, *339*, 269.
- [30] P. Roca-Cusachs, N. C. Gauthier, A. Del Rio, M. P. Sheetz, *Proc. Natl. Acad. Sci. U. S. A.* **2009**, *106*, 16245.
- [31] M. Morimatsu, A. H. Mekhdjian, A. C. Chang, S. J. Tan, A. R. Dunn, *Nano Lett.* **2015**, *15*, 2220.
- [32] K. R. Legate, R. Fässler, *J. Cell Sci.* **2009**, *122*, 187.
- [33] A. del Rio, R. Perez-Jimenez, R. Liu, P. Roca-Cusachs, J. M. Fernandez, M. P. Sheetz, *Science* **2009**, *323*, 638.
- [34] D. P. Felsenfeld, P. L. Schwartzberg, A. Venegas, R. Tse, M. P. Sheetz, *Nat. Cell Biol.* **1999**, *1*, 200.
- [35] A. Kostic, M. P. Sheetz, *Mol. Biol. Cell* **2006**, *17*, 2684.
- [36] D. Ilic, Y. Furuta, S. Kanazawa, N. Takeda, K. Sobue, N. Nakatsuji, S. Nomura, J. Fujimoto, M. Okada, T. Yamamoto, *Nature* **1995**, *377*, 539.

- [37] A. J. Maniotis, C. S. Chen, D. E. Ingber, *Proc. Natl. Acad. Sci. U. S. A.* **1997**, *94*, 849.
- [38] N. Wang, J. D. Tytell, D. E. Ingber, *Nat. Rev. Mol. Cell Biol.* **2009**, *10*, 75.
- [39] D.-H. Kim, S. B. Khatau, Y. Feng, S. Walcott, S. X. Sun, G. D. Longmore, D. Wirtz, *Sci. Rep.* **2012**, *2*, 555.
- [40] A. B. Chambliss, S. B. Khatau, N. Erdenberger, D. K. Robinson, D. Hodzic, G. D. Longmore, D. Wirtz, *Sci. Rep.* **2013**, *3*, 1087.
- [41] A. Livne, B. Geiger, *J. Cell Sci.* **2016**, *129*, 1293.
- [42] J. C. Friedland, M. H. Lee, D. Boettiger, *Science* **2009**, *323*, 642.
- [43] F. Kong, A. J. García, A. P. Mould, M. J. Humphries, C. Zhu, *J. Cell Biol.* **2009**, *185*, 1275.
- [44] E. A. Evans, R. Waugh, L. Melnik, *Biophys. J.* **1976**, *16*, 585.
- [45] E. Evans, K. Ritchie, R. Merkel, *Biophys. J.* **1995**, *68*, 2580.
- [46] N. Walter, C. Selhuber, H. Kessler, J. P. Spatz, *Nano Lett.* **2006**, *6*, 398.
- [47] M. Tanase, N. Biais, M. Sheetz, *Methods Cell Biol.* **2007**, *83*, 473.
- [48] P. Honarmandi, H. Lee, M. J. Lang, R. D. Kamm, *Lab Chip* **2011**, *11*, 684.
- [49] S. Romero, A. Quatela, T. Bornschlögl, S. Guadagnini, P. Bassereau, G. Tran Van Nhieu, *J. Cell Sci.* **2012**, *125*, 4999.
- [50] J. Helenius, C. P. Heisenberg, H. E. Gaub, D. J. Müller, *J. Cell Sci.* **2008**, *121*, 1785.
- [51] A. V. Taubenberger, D. W. Hutmacher, D. J. Müller, *Tissue Eng., Part B* **2014**, *20*, 40.
- [52] J. Friedrichs, K. R. Legate, R. Schubert, M. Bharadwaj, C. Werner, D. J. Müller, M. Benoit, *Methods* **2013**, *60*, 169.
- [53] K. Haase, A. E. Pelling, *J. R. Soc., Interface* **2015**, *12*.
- [54] M. Benoit, D. Gabriel, G. Gerisch, H. E. Gaub, *Nat. Cell Biol.* **2000**, *2*, 313.
- [55] M. A. Horton, M. L. Taylor, T. R. Arnett, M. H. Helfrich, *Exp. Cell Res.* **1991**, *195*, 368.
- [56] P. T. Lakkakorpi, M. A. Horton, M. H. Helfrich, E. K. Karhukorpi, H. K. Väänänen, *J. Cell Biol.* **1991**, *115*, 1179.
- [57] P. P. Lehenkari, M. A. Horton, *Biochem. Biophys. Res. Commun.* **1999**, *259*, 645.
- [58] A. Taubenberger, D. A. Cisneros, J. Friedrichs, P.-H. Puech, D. J. Müller, C. M. Franz, *Mol. Biol. Cell* **2007**, *18*, 1634.
- [59] F. Y. Li, S. D. Redick, H. P. Erickson, V. T. Moy, *Biophys. J.* **2003**, *84*, 1252.
- [60] X. Zhang, S. E. Craig, H. Kirby, M. J. Humphries, V. T. Moy, *Biophys. J.* **2004**, *87*, 3470.
- [61] R. Alon, S. W. Feigelson, E. Manevich, D. M. Rose, J. Schmitz, D. R. Overby, E. Winter, V. Grabovsky, V. Shinder, B. D. Matthews, M. Sokolovsky-Eisenberg, D. E. Ingber, M. Benoit, M. H. Ginsberg, *J. Cell Biol.* **2005**, *171*, 1073.
- [62] E. Kokkoli, S. E. Ochsenhirt, M. Tirrell, *Langmuir* **2004**, *20*, 2397.
- [63] R. I. Litvinov, J. S. Bennett, J. W. Weisel, H. Shuman, *Biophys. J.* **2005**, *89*, 2824.
- [64] D. J. Müller, J. Helenius, D. Alsteens, Y. F. Dufrene, *Nat. Chem. Biol.* **2009**, *5*, 383.
- [65] R. J. Owen, C. D. Heyes, D. Knebel, C. Röcker, G. U. Nienhaus, *Biopolymers* **2006**, *82*, 410.
- [66] M. J. Jacobs, K. Blank, *Chem. Sci.* **2014**, *5*, 1680.
- [67] A. Harris, P. Wild, D. Stopak, *Science* **1980**, *208*, 177.
- [68] J. Lee, M. Leonard, T. Oliver, A. Ishihara, K. Jacobson, *J. Cell Biol.* **1994**, *127*, 1957.

- [69] M. Dembo, Y.-L. Wang, *Biophys. J.* **1999**, *76*, 2307.
- [70] K. A. Beningo, M. Dembo, I. Kaverina, J. V. Small, Y.-l. Wang, *J. Cell Biol.* **2001**, *153*, 881.
- [71] S. A. Maskarinec, C. Franck, D. A. Tirrell, G. Ravichandran, *Proc. Natl. Acad. Sci. U. S. A.* **2009**, *106*, 22108.
- [72] W. R. Legant, J. S. Miller, B. L. Blakely, D. M. Cohen, G. M. Genin, C. S. Chen, *Nat. Methods* **2010**, *7*, 969.
- [73] R. J. Pelham, Y.-l. Wang, *Proc. Natl. Acad. Sci. U. S. A.* **1997**, *94*, 13661.
- [74] S. Khetan, M. Guvendiren, W. R. Legant, D. M. Cohen, C. S. Chen, J. A. Burdick, *Nat. Mater.* **2013**, *12*, 458.
- [75] J. L. Tan, J. Tien, D. M. Pirone, D. S. Gray, K. Bhadriraju, C. S. Chen, *Proc. Natl. Acad. Sci. U. S. A.* **2003**, *100*, 1484.
- [76] L. Trichet, J. Le Digabel, R. J. Hawkins, S. R. Vedula, M. Gupta, C. Ribault, P. Hersen, R. Voituriez, B. Ladoux, *Proc. Natl. Acad. Sci. U. S. A.* **2012**, *109*, 6933.
- [77] N. Q. Balaban, U. S. Schwarz, D. Riveline, P. Goichberg, G. Tzur, I. Sabanay, D. Mahalu, S. Safran, A. Bershadsky, L. Addadi, B. Geiger, *Nat. Cell Biol.* **2001**, *3*, 466.
- [78] C. Albrecht, K. Blank, M. Lalic-Mülthaler, S. Hirler, T. Mai, I. Gilbert, S. Schiffmann, T. Bayer, H. Clausen-Schaumann, H. E. Gaub, *Science* **2003**, *301*, 367.
- [79] C. H. Albrecht, H. Clausen-Schaumann, H. E. Gaub, *J. Phys.: Condens. Matter* **2006**, *18*, S581.
- [80] M. B. Viani, T. E. Schäffer, A. Chand, M. Rief, H. E. Gaub, P. K. Hansma, *J. Appl. Phys.* **1999**, *86*, 2258.
- [81] T. Strunz, K. Oroszlan, R. Schäfer, H. J. Güntherodt, *Proc. Natl. Acad. Sci. U. S. A.* **1999**, *96*, 11277.
- [82] J. Morfill, F. Kühner, K. Blank, R. A. Lugmaier, J. Sedlmair, H. E. Gaub, *Biophys. J.* **2007**, *93*, 2400.
- [83] K. Hatch, C. Danilowicz, V. Coljee, M. Prentiss, *Phys. Rev. E* **2008**, *78*, 011920.
- [84] M. Rief, H. Clausen-Schaumann, H. E. Gaub, *Nat. Struct. Mol. Biol.* **1999**, *6*, 346.
- [85] R. Krautbauer, M. Rief, H. E. Gaub, *Nano Lett.* **2003**, *3*, 493.
- [86] S. B. Smith, Y. Cui, C. Bustamante, *Science* **1996**, *271*, 795.
- [87] P. Cluzel, A. Lebrun, C. Heller, R. Lavery, J.-L. Viovy, D. Chatenay, F. Caron, *Science* **1996**, *271*, 792.
- [88] U. Bockelmann, B. Essevaz-Roulet, F. Heslot, *Phys. Rev. Lett.* **1997**, *79*, 4489.
- [89] P. M. Severin, X. Zou, H. E. Gaub, K. Schulten, *Nucleic Acids Res.* **2011**, *39*, 8740.
- [90] P. M. Severin, X. Zou, K. Schulten, H. E. Gaub, *Biophys. J.* **2013**, *104*, 208.
- [91] D. Ho, K. Falter, P. Severin, H. E. Gaub, *Anal. Chem.* **2009**, *81*, 3159.
- [92] D. Ho, C. Dose, C. H. Albrecht, P. Severin, K. Falter, P. B. Dervan, H. E. Gaub, *Biophys. J.* **2009**, *96*, 4661.
- [93] P. M. Severin, D. Ho, H. E. Gaub, *Lab Chip* **2011**, *11*, 856.
- [94] P. M. Severin, H. E. Gaub, *Small* **2012**, *8*, 3269.
- [95] K. Limmer, D. Aschenbrenner, H. E. Gaub, *Nucleic Acids Res.* **2013**, *41*, e69.
- [96] C. Dose, D. Ho, H. E. Gaub, P. B. Dervan, C. H. Albrecht, *Angew. Chem. Int. Ed.* **2007**, *46*, 8384.
- [97] K. Limmer, D. A. Pippig, D. Aschenbrenner, H. E. Gaub, *PLoS One* **2014**, *9*, e89626.

- [98] M. Otten, P. Wolf, H. E. Gaub, *Lab Chip* **2013**, *13*, 4198.
- [99] K. Blank, T. Mai, I. Gilbert, S. Schiffmann, J. Rankl, R. Zivin, C. Tackney, T. Nicolaus, K. Spinnler, F. Oesterhelt, M. Benoit, H. Clausen-Schaumann, H. E. Gaub, *Proc. Natl. Acad. Sci. U. S. A.* **2003**, *100*, 11356.
- [100] K. Blank, A. Lankenau, T. Mai, S. Schiffmann, I. Gilbert, S. Hirler, C. Albrecht, M. Benoit, H. E. Gaub, H. Clausen-Schaumann, *Anal. Bioanal. Chem.* **2004**, *379*, 974.
- [101] I. Gilbert, S. Schiffmann, S. Rubenwolf, K. Jensen, T. Mai, C. Albrecht, A. Lankenau, G. Beste, K. Blank, H. E. Gaub, H. Clausen-Schaumann, *Proteomics* **2004**, *4*, 1417.
- [102] D. Aschenbrenner, D. A. Pippig, K. Klamecka, K. Limmer, H. Leonhardt, H. E. Gaub, *PLoS One* **2014**, *9*, e115049.
- [103] U. Wienken, H. E. Gaub, *Biophys. J.* **2013**, *105*, 2687.
- [104] G. Neuert, C. H. Albrecht, H. E. Gaub, *Biophys. J.* **2007**, *93*, 1215.
- [105] M. J. Lang, P. M. Fordyce, S. M. Block, *J. Biol.* **2003**, *2*, 1.
- [106] M. J. Lang, P. M. Fordyce, A. M. Engh, K. C. Neuman, S. M. Block, *Nat. Methods* **2004**, *1*, 133.
- [107] H. Shroff, B. M. Reinhard, M. Siu, H. Agarwal, A. Spakowitz, J. Liphardt, *Nano Lett.* **2005**, *5*, 1509.
- [108] P. B. Tarsa, R. R. Brau, M. Barch, J. M. Ferrer, Y. Freyzon, P. Matsudaira, M. J. Lang, *Angew. Chem. Int. Ed.* **2007**, *46*, 1999.
- [109] H. Shroff, D. Sivak, J. J. Siegel, A. L. McEvoy, M. Siu, A. Spakowitz, P. L. Geissler, J. Liphardt, *Biophys. J.* **2008**, *94*, 2179.
- [110] C. Grashoff, B. D. Hoffman, M. D. Brenner, R. Zhou, M. Parsons, M. T. Yang, M. A. McLean, S. G. Sligar, C. S. Chen, T. Ha, M. A. Schwartz, *Nature* **2010**, *466*, 263.
- [111] D. R. Stabley, C. Jurchenko, S. S. Marshall, K. S. Salaita, *Nat. Methods* **2012**, *9*, 64.
- [112] X. Wang, T. Ha, *Science* **2013**, *340*, 991.
- [113] P.-G. de Gennes, *C. R. Acad. Sci., Ser. IV: Phys.* **2001**, *2*, 1505.
- [114] F. Chowdhury, I. T. S. Li, B. J. Leslie, S. Doganay, R. Singh, X. Wang, J. Seong, S.-H. Lee, S. Park, N. Wang, T. Ha, *Integr. Biol.* **2015**, *7*, 1265.
- [115] X. Wang, J. Sun, Q. Xu, F. Chowdhury, M. Roein-Peikar, Y. Wang, T. Ha, *Biophys. J.* **2015**, *109*, 2259.
- [116] M. Roein-Peikar, Q. Xu, X. Wang, T. Ha, *Phys. Rev. X* **2016**, *6*, 011001.
- [117] F. Chowdhury, I. T. S. Li, T. T. M. Ngo, B. J. Leslie, B. C. Kim, J. E. Sokoloski, E. Weiland, X. Wang, Y. R. Chemla, T. M. Lohman, T. Ha, *Nano Lett.* **2016**, *16*, 3892.
- [118] Z. Wan, X. Chen, H. Chen, Q. Ji, Y. Chen, J. Wang, Y. Cao, F. Wang, J. Lou, Z. Tang, W. Liu, *eLife* **2015**, *4*, e06925.
- [119] Y. Liu, L. Blanchfield, V. P.-Y. Ma, R. Andargachew, K. Galior, Z. Liu, B. Evavold, K. Salaita, *Proc. Natl. Acad. Sci. U. S. A.* **2016**.
- [120] X. Wang, Z. Rahil, I. T. S. Li, F. Chowdhury, D. E. Leckband, Y. R. Chemla, T. Ha, *Sci. Rep.* **2016**, *6*, 21584.
- [121] F. M. Watt, W. T. S. Huck, *Nat. Rev. Mol. Cell Biol.* **2013**, *14*, 467.
- [122] R. K. Das, V. Gocheva, R. Hammink, O. F. Zouani, A. E. Rowan, *Nat. Mater.* **2016**, *15*, 318.
- [123] M. K. Lee, J. Park, X. Wang, M. Roein-Peikar, E. Ko, E. Qin, J. Lee, T. Ha, H. Kong, *Chem. Commun.* **2016**, *52*, 4757.

- [124] C. Jurchenko, Y. Chang, Y. Narui, Y. Zhang, Khalid S. Salaita, *Biophys. J.* **2014**, *106*, 1436.
- [125] Y. Chang, Z. Liu, Y. Zhang, K. Galior, J. Yang, K. Salaita, *J. Am. Chem. Soc.* **2016**, *138*, 2901.
- [126] Y. Liu, K. Yehl, Y. Narui, K. Salaita, *J. Am. Chem. Soc.* **2013**, *135*, 5320.
- [127] Y. Liu, R. Medda, Z. Liu, K. Galior, K. Yehl, J. P. Spatz, E. A. Cavalcanti-Adam, K. Salaita, *Nano Lett.* **2014**, *14*, 5539.
- [128] M. Morimatsu, A. H. Mekhdjian, A. S. Adhikari, A. R. Dunn, *Nano Lett.* **2013**, *13*, 3985.
- [129] B. L. Blakely, C. E. Dumelin, B. Trappmann, L. M. McGregor, C. K. Choi, P. C. Anthony, V. K. Duesterberg, B. M. Baker, S. M. Block, D. R. Liu, C. S. Chen, *Nat. Methods* **2014**, *11*, 1229.
- [130] Y. Zhang, C. Ge, C. Zhu, K. Salaita, *Nat. Commun.* **2014**, *5*.
- [131] K. Galior, Y. Liu, K. Yehl, S. Vivek, K. Salaita, *Nano Lett.* **2016**, *16*, 341.
- [132] M. T. Woodside, W. M. Behnke-Parks, K. Larizadeh, K. Travers, D. Herschlag, S. M. Block, *Proc. Natl. Acad. Sci. U. S. A.* **2006**, *103*, 6190.
- [133] M. Rief, M. Gautel, F. Oesterhelt, J. M. Fernandez, H. E. Gaub, *Science* **1997**, *276*, 1109.
- [134] M. Carrion-Vazquez, A. F. Oberhauser, S. B. Fowler, P. E. Marszalek, S. E. Broedel, J. Clarke, J. M. Fernandez, *Proc. Natl. Acad. Sci. U. S. A.* **1999**, *96*, 3694.
- [135] F. Meng, T. M. Suchyna, F. Sachs, *FEBS J.* **2008**, *275*, 3072.
- [136] F. Meng, T. M. Suchyna, E. Lazakovitch, R. M. Gronostajski, F. Sachs, *Cell. Mol. Bioeng.* **2011**, *4*, 148.
- [137] S. Iwai, T. Q. Uyeda, *Proc. Natl. Acad. Sci. U. S. A.* **2008**, *105*, 16882.
- [138] S. Iwai, T. Q. Uyeda, *Cytometry A* **2010**, *77*, 743.
- [139] F. Meng, F. Sachs, *J. Cell Sci.* **2011**, *124*, 261.
- [140] F. Meng, F. Sachs, *J. Cell Sci.* **2012**, *125*, 743.
- [141] K. Austen, P. Ringer, A. Mehlich, A. Chrostek-Grashoff, C. Kluger, C. Klingner, B. Sabass, R. Zent, M. Rief, C. Grashoff, *Nat. Cell Biol.* **2015**, *17*, 1597.
- [142] J. Rahimzadeh, F. Meng, F. Sachs, J. Wang, D. Verma, S. Z. Hua, *Am. J. Physiol. Cell Physiol.* **2011**, *301*, C646.
- [143] G. Zocchi, *Annu. Rev. Biophys.* **2009**, *38*, 75.
- [144] M. Otten, W. Ott, M. A. Jobst, L. F. Milles, T. Verdorfer, D. A. Pippig, M. A. Nash, H. E. Gaub, *Nat. Methods* **2014**, *11*, 1127.
- [145] D. Verma, F. Meng, F. Sachs, S. Z. Hua, *Cell Adhes. Migr.* **2015**, *9*, 432.
- [146] K. Suffoletto, N. Ye, F. Meng, D. Verma, S. Z. Hua, *J. Biomech.* **2015**, *48*, 627.
- [147] N. Ye, D. Verma, F. Meng, M. W. Davidson, K. Suffoletto, S. Z. Hua, *Exp. Cell Res.* **2014**, *327*, 57.
- [148] M. D. Brenner, R. Zhou, D. E. Conway, L. Lanzano, E. Gratton, M. A. Schwartz, T. Ha, *Nano Lett.* **2016**, *16*, 2096.
- [149] C.-W. Chang, S. Kumar, *J. Cell Sci.* **2013**, *126*, 3021.
- [150] P. Hernandez-Varas, U. Berge, J. G. Lock, S. Stromblad, *Nat. Commun.* **2015**, *6*.
- [151] N. Borghi, M. Sorokina, O. G. Shcherbakova, W. I. Weis, B. L. Pruitt, W. J. Nelson, A. R. Dunn, *Proc. Natl. Acad. Sci. U. S. A.* **2012**, *109*, 12568.

- [152] D. Cai, S. C. Chen, M. Prasad, L. He, X. Wang, V. Choesmel-Cadamuro, J. K. Sawyer, G. Danuser, D. J. Montell, *Cell* **2014**, *157*, 1146.
- [153] D. E. Conway, M. T. Breckenridge, E. Hinde, E. Gratton, C. S. Chen, M. A. Schwartz, *Curr. Biol.* **2013**, *23*, 1024.
- [154] M. Krieg, A. R. Dunn, M. B. Goodman, *Nat. Cell Biol.* **2014**, *16*, 224.
- [155] M. Kelley, J. Yochem, M. Krieg, A. Calixto, M. G. Heiman, A. Kuzmanov, V. Meli, M. Chalfie, M. B. Goodman, S. Shaham, A. Frand, D. S. Fay, *eLife* **2015**, *4*, e06565.
- [156] M. J. Paszek, C. C. DuFort, O. Rossier, R. Bainer, J. K. Mouw, K. Godula, J. E. Hudak, J. N. Lakins, A. C. Wijekoon, L. Cassereau, M. G. Rubashkin, M. J. Magbanua, K. S. Thorn, M. W. Davidson, H. S. Rugo, J. W. Park, D. A. Hammer, G. Giannone, C. R. Bertozzi, V. M. Weaver, *Nature* **2014**, *511*, 319.
- [157] H. Zohar, C. L. Hetherington, C. Bustamante, S. J. Muller, *Nano Lett.* **2010**, *10*, 4697.
- [158] S. Dutta, B. A. Armitage, Y. L. Lyubchenko, *Biochemistry* **2016**, *55*, 1523.
- [159] H. Dietz, M. Rief, *Proc. Natl. Acad. Sci. U. S. A.* **2004**, *101*, 16192.
- [160] M. Mosayebi, A. A. Louis, J. P. K. Doye, T. E. Ouldridge, *ACS Nano* **2015**, *9*, 11993.
- [161] G. I. Bell, *Science* **1978**, *200*, 618.
- [162] E. Evans, K. Ritchie, *Biophys. J.* **1997**, *72*, 1541.
- [163] E. Evans, *Annu. Rev. Biophys. Biomol. Struct.* **2001**, *30*, 105.
- [164] S. R. Deshpande, R. Hammink, R. K. Das, F. H. T. Nelissen, K. G. Blank, A. E. Rowan, H. A. Heus, *Adv. Funct. Mater.* **2016**, doi:10.1002/adfm.201602461.

Author biographies



Melis Goktas is currently a PhD student at the Max Planck Institute of Colloids and Interfaces, Potsdam (Germany). She received her BSc degree in Bioengineering from Ege University and MSc degree in Materials Science and Nanotechnology from the National Nanotechnology Research Center (UNAM), Bilkent University (Turkey). Her research interests include single-molecule force spectroscopy, mechanobiology and cell-ECM interactions.



Kerstin Blank received her PhD degree in Biophysics from Ludwig-Maximilians University in Munich (Germany), in 2006. After two short postdoctoral stays at the University of Strasbourg (France) and the University of Leuven (Belgium), she became assistant professor at Radboud University (Nijmegen, The Netherlands) in 2009. In 2014 she moved to the Max Planck Institute of Colloids and Interfaces in Potsdam (Germany) where she is leading the Max Planck Research Group 'Mechano(bio)chemistry'. Her research interests combine her backgrounds in biochemistry and single-molecule biophysics with the goal of developing molecular force sensors for biological and materials science applications.